AD NUMBER

AD816286

LIMITATION CHANGES

TO:

Approved for public release; distribution is unlimited.

FROM:

Distribution authorized to DoD only; Administrative/Operational Use; 12 MAY 1967. Other requests shall be referred to Naval Air Development Center, Warminster PA 18974.

AUTHORITY

USNADC ltr, 28 Aug 1974

V 0501U/2.510

AN INTRODUCTION TO LAUNCH ACCEPTABILITY REGIONS

12 May 1967

Veda Report V 0501U/2.510

AN INTRODUCTION TO LAUNCH ACCEPTABILITY REGIONS

12 May 1967

Performed Under

Contract N 62269-67-C-0418

for

U. S. Naval Air Development Center
Johnsville
Warminster Pennsylvania 18974

by

Veda Incorporated
15 Research Drive
Ann Arbor, Michigan 48103

veda
INCORPORATED

PREFACE

This study was performed by Veda Incorporated for the U. S. Naval Air Development Center under Contract N 62269-67-C-0418. This report, which is submitted in fulfillment of that contract, is intended to be a general orientation in the subject of air-to-air missile launch acceptability regions.

veda
INCORPORATED

ABSTRACT

This report is intended to be a general orientation in the subject of air-to-air missile Launch Acceptability Region (LAR) diagrams. To this end a qualitative and quantative description of the various weapon system performance characteristics pertinent to the determination of LAR diagrams is presented. Each of the characteristics are treated separately with a discussion including the general nature of the characteristic, LAR regions where it can be expected to apply and where possible, equations describing its influence on LAR diagrams. Where examples of LAR diagrams and system performance characteristics have been presented they have been made as specific as possible without requiring security classification.

The LAR characteristics and limiting factors discussed in this report, may be determined with a three-dimensional, five-degree of freedom, non-linear trim aerodynamic digital computer simulation. Information concerning this simulation may be obtained by contracting the AWRD department of the U.S. Naval Air Development Center, Johnsville, Warminster, Pennsylvania 18974.

veda
INCORPORATED

TABLE OF CONTENTS

TABLE OF CONTENTS (CONT.)

vedа INCORPORATED

LIST OF ILLUSTRATIONS

veda INCORPORATED

LIST OF ILLUSTRATIONS (CONT.)

veda
INCORPORATED 44

SECTION 1.0

INTRODUCTION

In order for an air-to-air homing missile to execute an intercept against a target, it must meet three basic requirements. First, the missile homing guidance system must be able to track the target. Secondly, the missile must be able to travel from its launch point to the intercept point. And finally, it must arrive at the intercept point with sufficient maneuverability to reduce the final miss distance to within the lethal radius of its warhead.

This report discusses the various features of an air-to-air missile that implement the above requirements, and their effects on its performance. A significant measure of an air-to-air weapon system's performance is its Launch Acceptability Region (LAR) diagram. This report is intended to be a general orientation in the subject of LAR diagrams. To this end the fundamental problem of missile guidance is discussed and LAR diagrams are defined in Section 2.0. Later sections not only specify some of the weapon system constraints that affect a LAR diagram, but also illustrate how they influence its shape. Where applicable, procedures are presented for the calculation of these factors for use in LAR determination. Finally in Section 7.0 the procedures and discussion, presented in the previous sections, are summarized to make available a ready reference of these factors.

veda

SECTION 2.0

FUNDAMENTAL CONSIDERATIONS

This section discusses some of the fundamental problems of air-to-air missile guidance both to familiarize the reader with these fundamentals and also to provide background information for the following sections. Specifically the following items are discussed:

1. Homing guidance techniques
2. Guidance phases of air-to-air missiles
3. Navigation laws for air-to-air missiles
4. Launch Acceptability Region (LAR) diagrams

2.1 HOMING GUIDANCE TECHNIQUES

Most contemporary air-launched guided missiles incorporate a target seeker into the missile itself; such guidance systems are termed "homing." Basically this means that the missile itself is able to process target information directly and command itself to "home" on the target. Homing guidance systems fall under one of three general types:

1. Active Homing
2. Passive Homing
3. Semi-Active Homing

A specific missile may, however, employ combinations of these three basic types. For example, the control of a missile may involve several guidance phases, each of which employ a different homing technique.

The first basic type of homing guidance is active homing and is illustrated in Figure 2.1a. In this type of guidance system the missile itself carries both the source of energy by which it illuminates the target (transmitter), and a receiver to receive the energy reflected from the target. Because of the severe size, weight and volume constraints placed on the missile, active homing guidance is usually employed only on short to medium range missiles (launch ranges to approximately ten nautical miles.)

veda INCORPORATED वेद

BASIC GUIDANCE HOMING TECHNIQUES

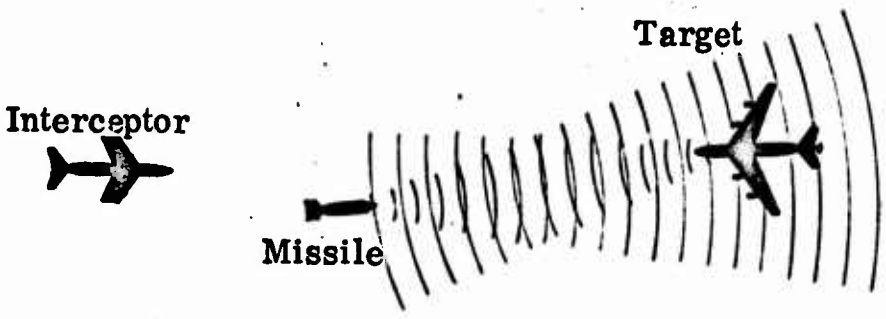

Active

Figure 2.1a

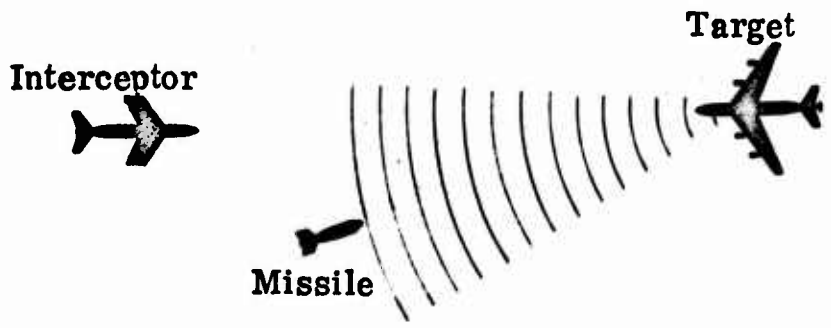

Passive

Figure 2.1b

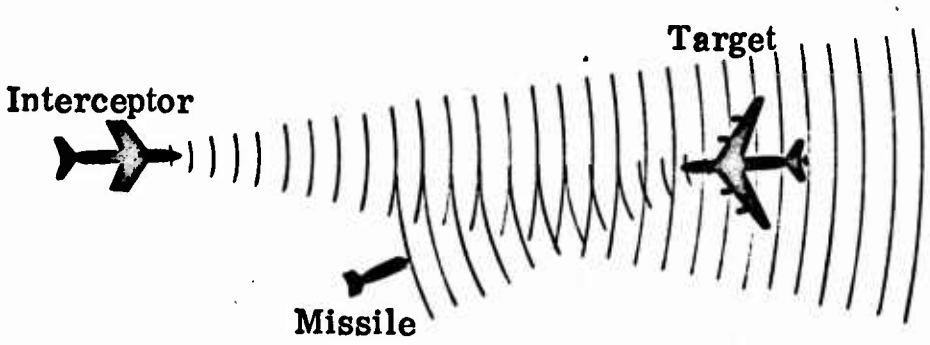

Semi-Active

Figure 2.1c

In the second basic type of homing guidance the missile "homes" on the energy emitted by the target. This type of guidance is termed passive homing and is illustrated in Figure 2.1 b. Because of the dependence on the target as the source of a guidance signal and also because of the necessity for all-weather performance, passive homing missiles are usually characterized by rather short launch ranges.

In a semiactive homing guidance system the target is illuminated by a source of energy that is located at a distance from the missile. A portion of this energy is scattered by the target and is detected and tracked by a receiver aboard the missile. As illustrated in Figure 2.1c, air-launched semiactive homing missiles usually incorporate the source of energy by which the target is illuminated into the parent aircraft or interceptor from which the missile is launched.

2.2 GUIDANCE PHASES OF AIR-TO-AIR MISSILES

Long range air-launched guided missiles are characterized by four distinct guidance phases:

1. Launch and Separation Phase
2. Midcourse Phase
3. Terminal Phase

The first phase of the flight extends from launch until the missile control system is activated. During this time the missile is separated from its launcher and its rocket motor ignites. Since one of the most important considerations during this phase is to ensure the safe separation of the missile from the launching aircraft, the missile control system must not be activated until the missile is clear of the interceptor. The Launch and Separation Phase of contemporary air-to-air missiles usually lasts from one to four seconds.

It is desirable to have the launch phase and separation phase as short as possible, because throughout these phases the missile's guidance system is not activated and it is operating without direct feedback from the target. Without this feedback a number of errors may build up which could prevent the missile from successfully acquiring the target when its guidance system is finally activated. These errors include trajectory errors due to launch perturbations, seeker head pointing errors due to component drifts, and unpredictable geometrical variations due to target maneuvers. On the other hand, though, a delay in target acquisition (and subsequent guidance commands) is desirable so that the missile may reach a position from which it can maneuver without endangering the launch aircraft.

The separation phase concludes and the mid-course phase begins when the missile acquires the target and begins to track it. In order to make this report as general as possible it will be assumed that during this phase the missile employs a semiactive radar homing guidance technique. This phase of the missile trajectory is discussed in detail in Sections 4.1.2 and 6.2.

The midcourse phase of flight ends and the terminal phase begins when the missile reaches the vicinity of the target. For purposes of this report it will be assumed that the missile employs an active radar homing guidance technique during the terminal phase.

2.3 NAVIGATION LAWS FOR AIR-TO-AIR MISSILES

This section presents a discussion of two typical navigation laws for purposes of illustrating the effect that the navigation law has on the trajectory and performance of an air-to-air missile. The two navigation laws are: Proportional Navigation and Deviated Pursuit. The interested reader is referred to reference 1 for a discussion of various other missile navigation laws.

2.3.1 Proportional Navigation

The purpose of a homing guidance system is to fly the missile to a collision (or near miss) with a target. The optimum trajectory to accomplish this is a straight line from the launch point to the "impact" point. For a constant speed missile and target the missile-to-target line-of-sight (LOS) will remain at a constant bearing throughout the missile flight. If missile speed varies, constant true bearing guidance commands the missile to fly such that the LOS remains spatially constant. This technique was used on early missiles but was found to be overly demanding on the missile control systems. This difficulty led to the development of proportional navigation.

To understand the kinematic relationships upon which proportional navigation is based, consider the geometry shown in Figure 2.2.

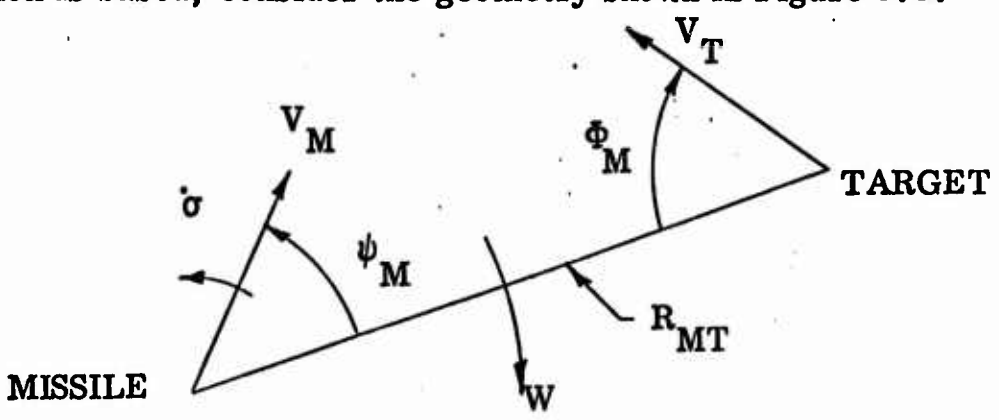

Guidance Geometry

Figure 2.2

The spatial rotation rate of the LOS is given by:

$$W = \frac{V_M \sin \psi_M - V_T \sin \Phi_M}{R_{MT}} \qquad (2.1)$$

Where

W = Rotation Rate of Missile-to-Target Line-of-Sight in Space

V_M = Missile Velocity

V_T = Target Velocity

ψ_M = Spatial Angle Between Missile Velocity Vector and Missile-to-Target LOS

Φ_M = Spatial Angle Between Target Velocity and Missile-to-Target LOS

R_{MT} = Missile-to-Target Range

If the LOS rate (W) is controlled in such a way that it is essentially zero, Equation 2.1 reduces to

$$V_M \sin \psi_M = V_T \sin \Phi_M \qquad (2.2)$$

Thus, if the rotation rate of the LOS is zero the components of missile and target velocity normal to the LOS will be equal. It is clear from Figure 2.2 that if the relation in Equation 2.2 is maintained, the LOS can only become shorter. Thus, an impact between the missile and target is assured.

If the speed of the missile is constant, the missile will travel in a straight line and intercept the target in minimum time. The problem with boost-glide missiles, however, is that they do not fly at constant speed. Because of this (as well as other factors which will be mentioned later) some means must be used to control the orientation of the missile velocity vector . As the LOS rotates in space so should the missile velocity vector. In fact it seems reasonable that the commanded rotation rate of the velocity vector should be proportional to the rotation rate of the LOS. This is the basis for proportional navigation and will yield direct control over the LOS rate and insure that the relation in Equation 2.2 in maintained.

veda INCORPORATED

In order to make the rotation rate of the missile velocity vector proportional to the LOS rotation rate, then, a relationship of the following form must be developed:

$$\dot{\sigma} = K_1 W \qquad (2.3)$$

Where

$\dot{\sigma}$ = Spatial rotation rate of missile velocity vector

K_1 = Velocity modified guidance gain for proportional navigation

It is known from kinematics that $\dot{\sigma}$ is governed by the equation

$$\dot{\sigma} = \frac{N_c}{V_M} \qquad (2.4)$$

Where

N_c = Lateral acceleration normal to V_M (See Figure 2.3)

Now in order to produce the $\dot{\sigma}$ called for in Equation 2.3, a force normal to the missile velocity must be produced. Combining Equations 2.3 and 2.4, yields:

$$N_c = K_1 V_M W \qquad (2.5)$$

Equation 2.5 defines what is known as the "Classical Proportional Navigation Law". The quantities V_M and W on the right side of Equation 2.5 are measured by the missile's guidance system, and are used to produce an acceleration command in the autopilot which in turn produces N_c.

In practice Equation 2.5 is not mechanized exactly because it is difficult to generate an acceleration which is normal to the missile velocity vector. Instead an acceleration is generated normal to the missile body axis. (See Figure 2.3). The difference is relatively minor in most applications and can be ignored. It has also been found that the V_M factor on the right side of Equation 2.5 can be assumed constant with little noticeable change in performance if the proper value of K_1 is selected.

The final result is a navigation law which is of the form:

$$N_{cn} = KW \qquad (2.6)$$

Where

N_{cn} = Lateral Acceleration normal to the missile body axis (See Figure 2.3)

K = Navigation Gain

MISSILE ACCELERATION GEOMETRY

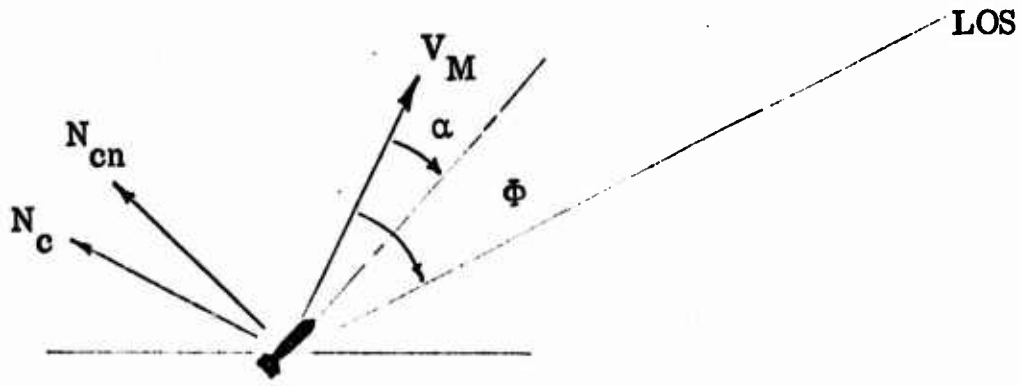

Figure 2.3

Equation 2.6 defines what will be termed "proportional navigation" in the remaining sections of this report. For analysis purposes it is convenient to resolve Equation 2.6 into components in the slant plane * and vertical plane, thus,

$$N_{cs} = KW_s \qquad (2.7)$$

$$N_{cv} = KW_v \qquad (2.8)$$

*Slant planes are planes containing the missile target line-of-sight or the interceptor and target line-of-sight and which are normal to the vertical plane. (See Figure 2.4).

veda INCORPORATED

MISSILE TARGET SLANT PLANE GEOMETRY

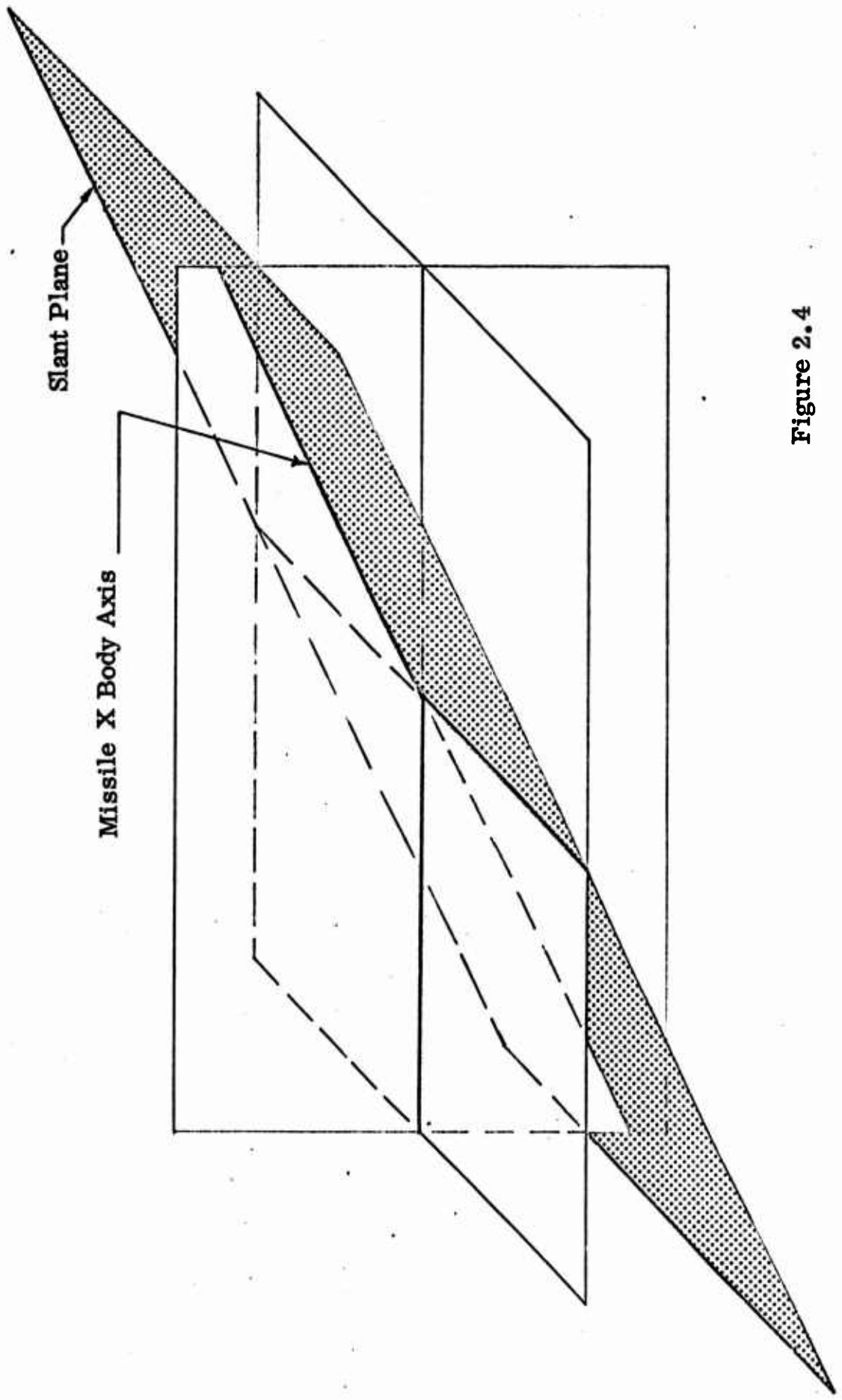

Figure 2.4

veda INCORPORATED

N_{cs} = Lateral slant plane acceleration command (normal to missile body axis)

N_{cv} = Lateral vertical plane acceleration command (normal to missile body axis)

K = Navigation gain

W_v = Vertical plane component of LOS rate

W_s = Slant plane component of LOS rate

Projections of typical trajectory that results when proportional navigation is employed as the guidance law for a long range missile are illustrated in Figure 2.5 a & b.

2.3.2 Deviated Pursuit Guidance

Deviated pursuit guidance is a guidance law that attempts to maintain a constant angle (lead angle) between the missile x-axis and the missile-to-target LOS. It may be stated in mathematical form as

$$N_{cs} = - C (G_{sc} - G_s) \qquad (2.9)$$

Where

N_{cs} = Lateral Acceleration normal to missile body axis in slant plane

G_s = Slant plane projection of missile to target look angle (gimbal angle)

G_{sc} = Commanded slant plane lead angle

C = Navigation Gain

Unlike proportional navigation, deviated pursuit causes the missile-to-target LOS to rotate during the missile's flight rather than remain fixed.

The rotation rate of the LOS is controlled by the selection of the commanded

veda INCORPORATED

PROPORTIONAL NAVIGATION TRAJECTORIES

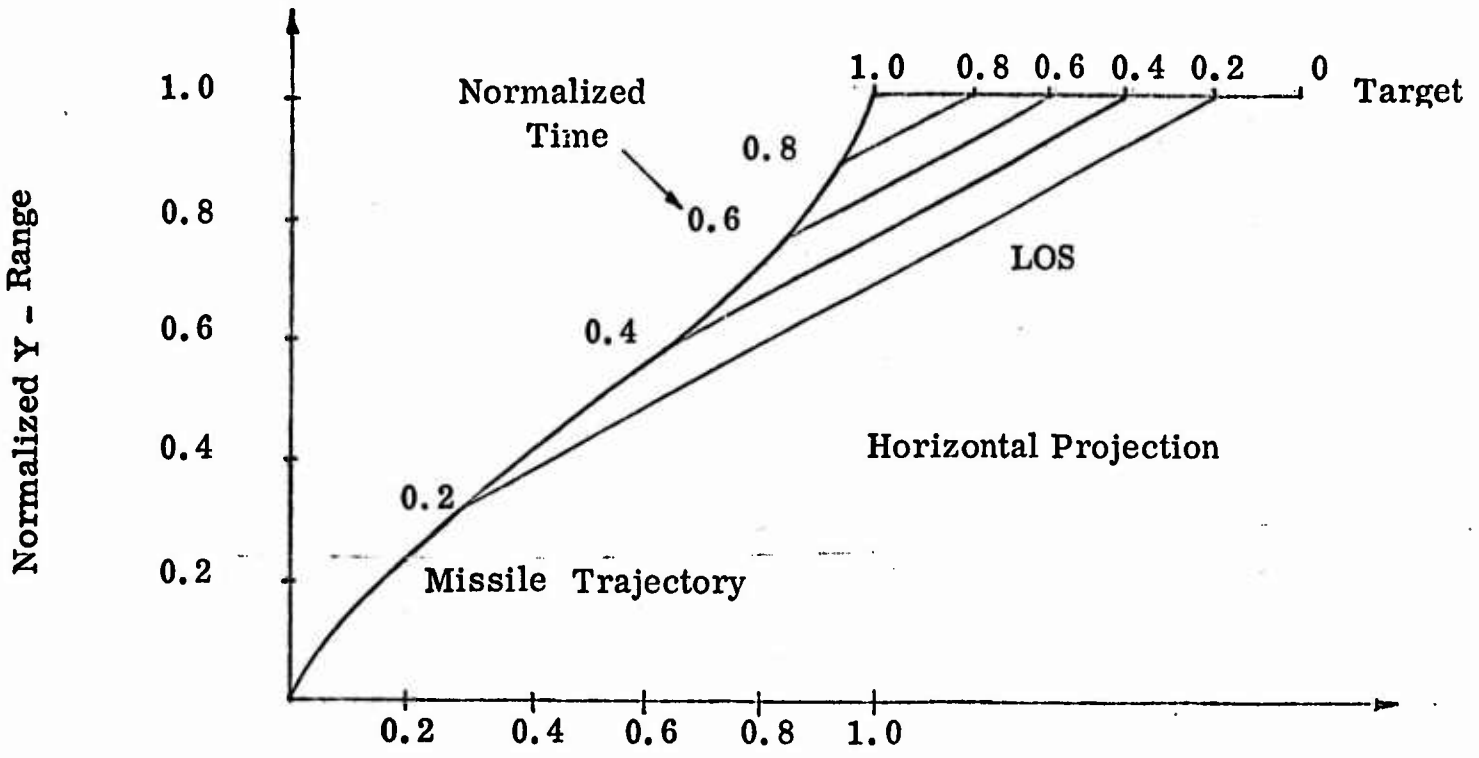

Figure 2.5 a

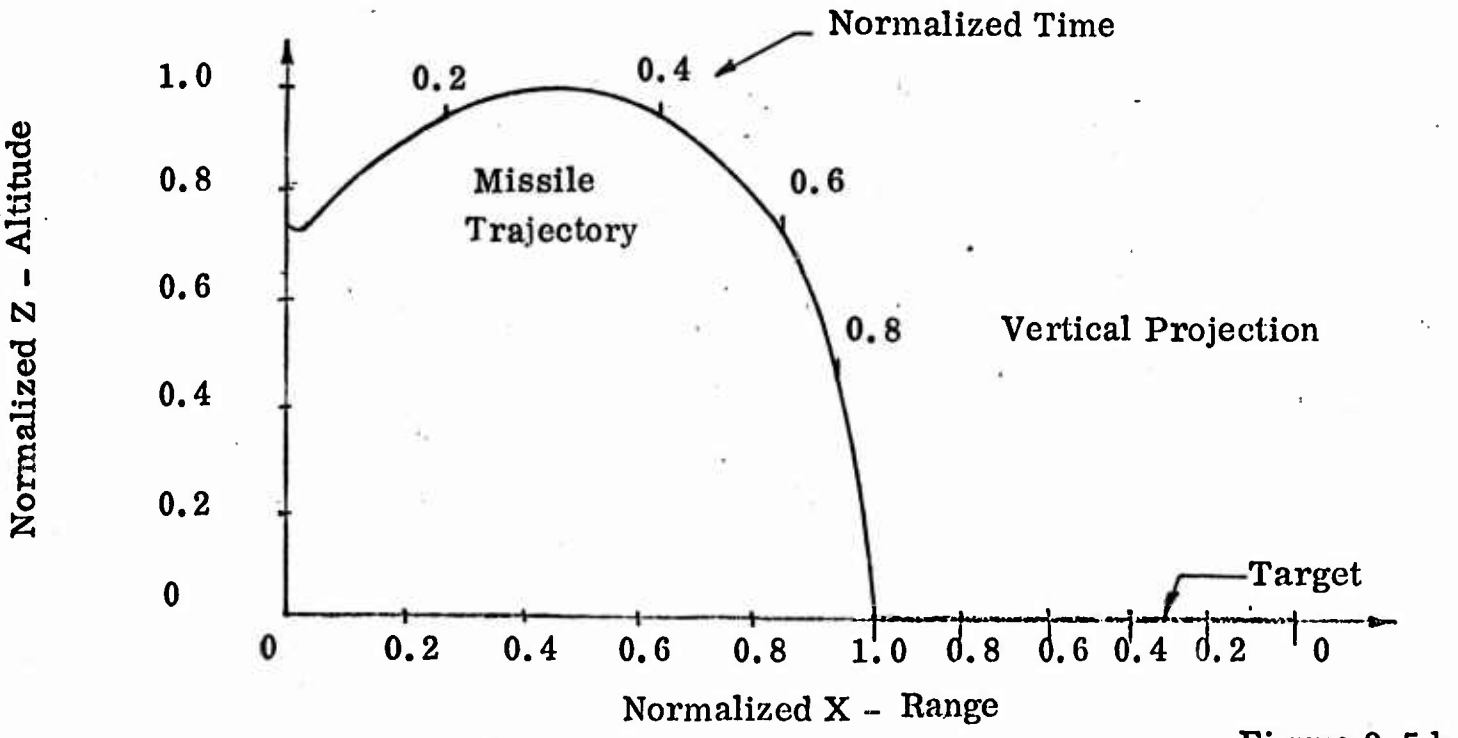

Figure 2.5 b

lead angle (G_{sc}) and can be made to cause the target aspect angle (angle between the target velocity vector and interceptor-target LOS) to decrease with time. It is evident from the horizontal plane projection of a typical trajectory illustrated in Figure 2.6 that deviated pursuit causes the missile to approach the target from a more frontal position for the terminal intercept.

Envelopes of acceptable values of lead angle (G_{sc}) take the shape as illustrated in Figure 2.7.

2.4 LAUNCH ACCEPTABILITY REGION (LAR) DIAGRAMS

A launch acceptability region (LAR) is a graphical means of illustrating the maximum performance of a missile system. It is defined to be that region of space about the target (projected on a horizontal plane containing the target) within which a missile can be launched with a high probability of successfully intercepting the target. Intercept, as used here means that, in the absence of internally or externally generated guidance perturbations, the missile will approach the target to within a required distance. If the missile is launched from a point outside the LAR diagram, the performance limit of some part of the weapon system will be exceeded and an intercept will not be possible.

A LAR diagram is plotted in polar coordinates with the target located at the origin at the instant of missile launch, and is generated by determining the maximum (and minimum) launch range at which an intercept is possible for a given initial aspect angle (angle between the interceptor target line-of-sight and the target velocity vector). The locus of points resulting from varying this aspect angle then forms the LAR diagram (See Figure 2.8). Note that a given LAR diagram is defined only at the instant of missile launch and is valid for this time only.

A LAR diagram for a constant velocity, non-maneuvering target is specified by a set of attack conditions such as missile launch altitude and velocity and target altitude and velocity. The boundaries of a LAR diagram are generated by determining each of the constraints that may limit the ability of a missile to intercept the target. Although a multitude of missile system parameters act to determine the boundaries of a LAR, the limitations on missile launch range may be divided into two basic categories:

1. Prelaunch Geometric Constraints

2. Postlaunch Constraints

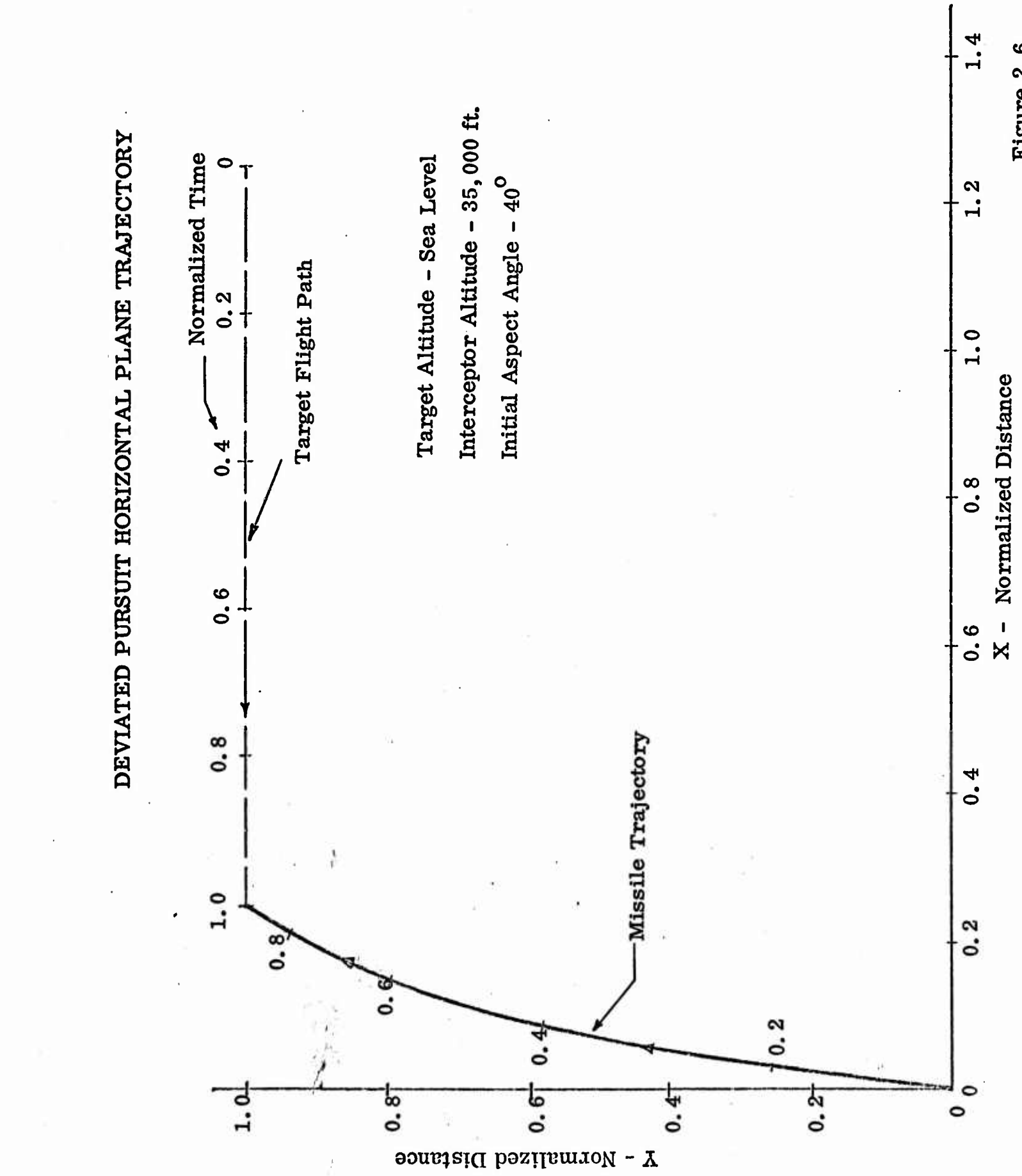
DEVIATED PURSUIT HORIZONTAL PLANE TRAJECTORY
Normalized Time
0.4
0.2
0
Target Flight Path
Target Altitude - Sea Level
Interceptor Altitude - 35,000 ft.
Initial Aspect Angle - 40°
Missile Trajectory
Y - Normalized Distance
X - Normalized Distance
1.0
0.8
0.6
0.4
0.2
0
1.4
1.2

Figure 2.6

veda INCORPORATED

LEAD ANGLE OPERATING ENVELOPE
DEVIATED PURSUIT GUIDANCE

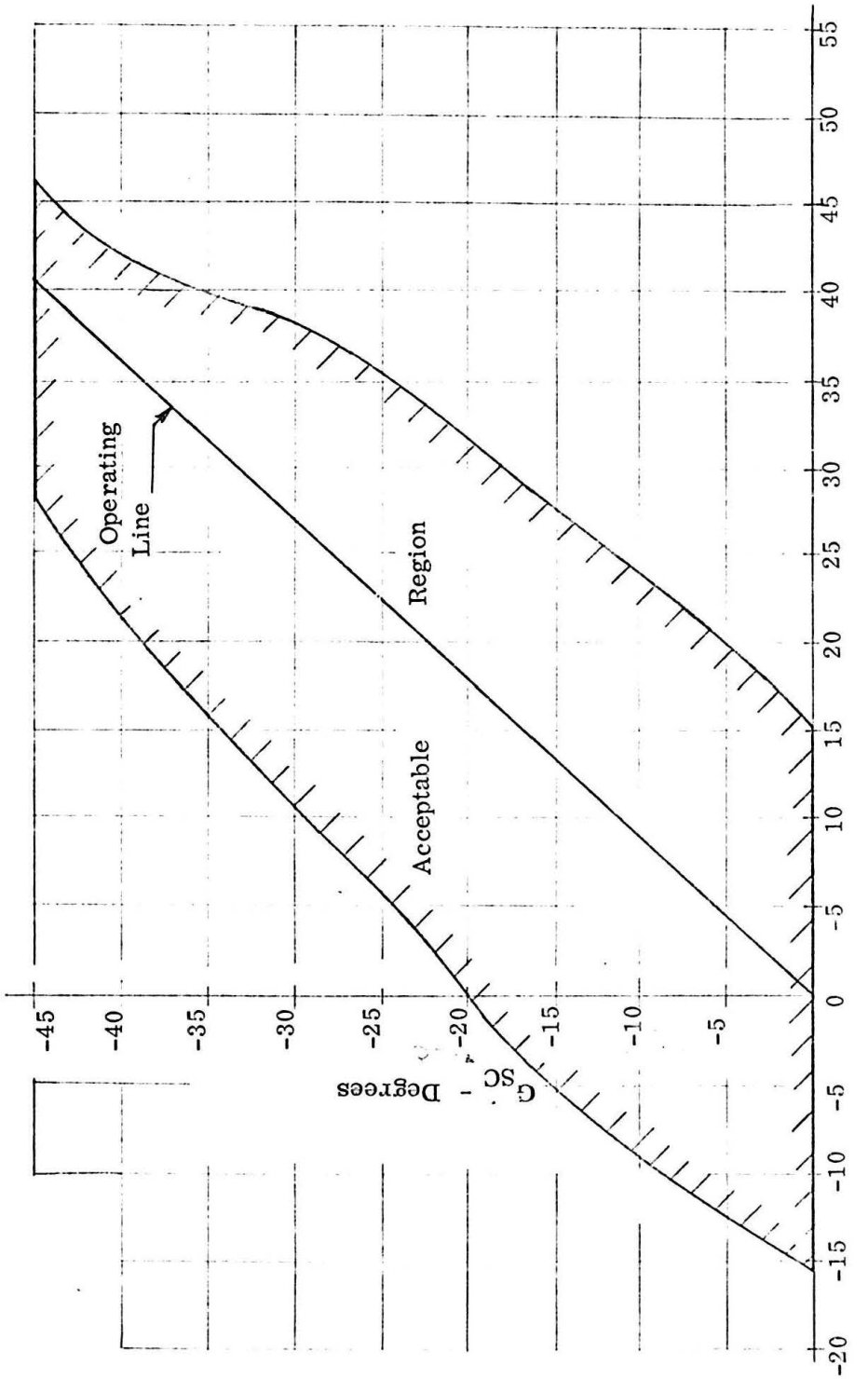

Figure 2.7

TYPICAL LAR DIAGRAM

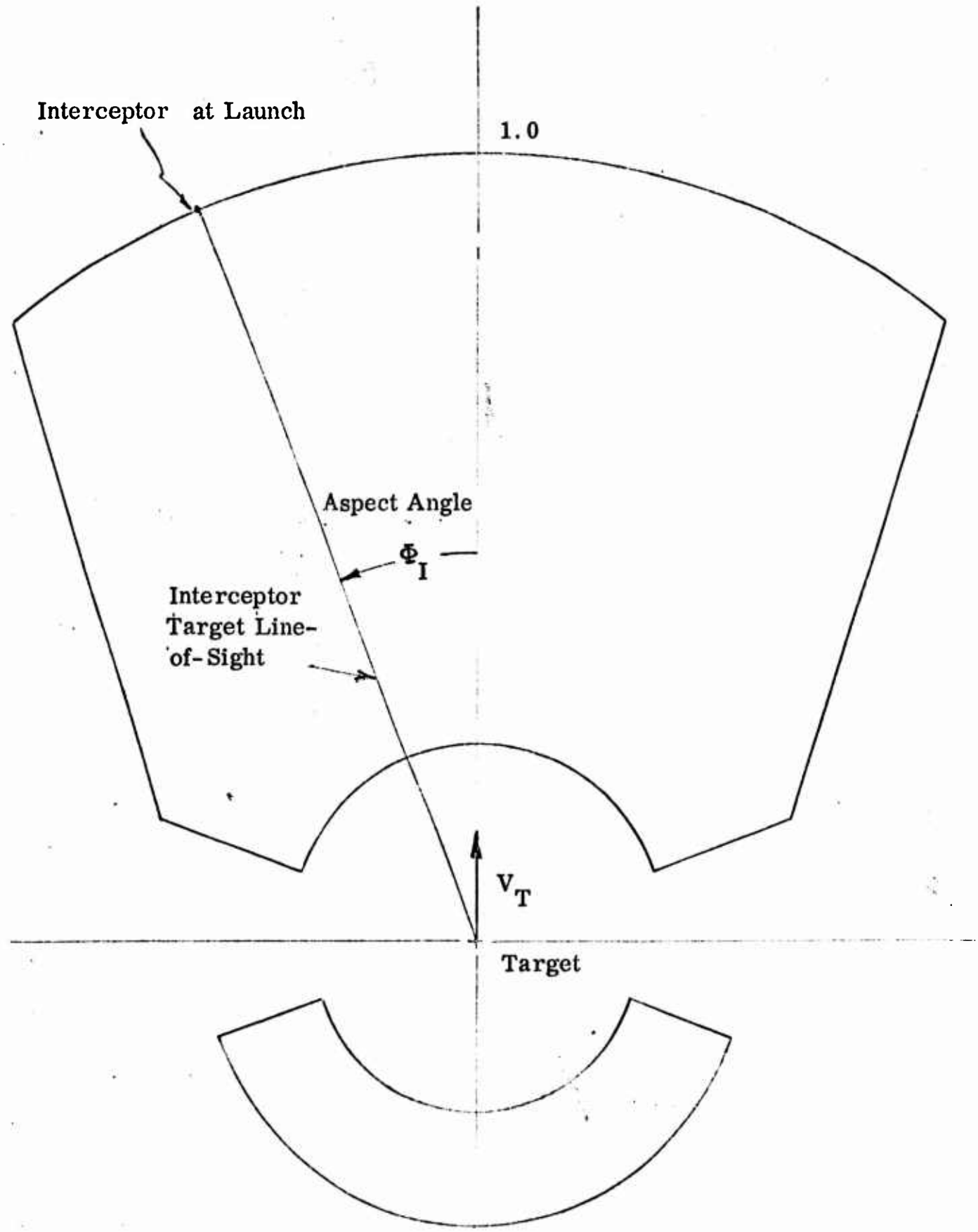

Figure 2.8

Prelaunch geometric constraints are due to the gimbal limits of the interceptor radar and the missile radar seeker. These parameters act to limit the minimum launch range of the missile and their effects on a LAR diagram is easily predicted, (subject to certain assumptions). Prelaunch geometric constraints are discussed in Section 3.0.

Postlaunch limiting factors, although easily identified, are somewhat difficult to predict. This is because the relationships between the various missile system parameters are, in general, time varying and non-linear. Postlaunch limiting factors may further be divided into three sub-categories:

1. Aerodynamic Constraints
2. Guidance System Constraints
3. Geometric Constraints

The effect of postlaunch constraints is to limit both the maximum and minimum LAR boundaries as well as the sides of the LAR. These effects are generally not amenable to linear analytical treatment and, except for isolated situations, must be investigated with the aid of both analog and digital computers. Postlaunch limiting factors are further discussed in Section 4.0, 5.0 and 6.0.

SECTION 3.0

PRELAUNCH GEOMETRIC CONSTRAINTS

Since the target must be within the gimbal angle or look angle of both the interceptor and the missile at the time of launch, then a portion of the potential launch acceptability region will be limited because of constraints on the interceptor and/or missile gimbal angles. In general the gimbal angle limits on the interceptor are not the same as those on the missile. If this is true then the portion of the LAR that is limited by gimbal angle constraints will be dictated by the smaller of either the interceptor or missile gimbal limits. The portion of the LAR limited by gimbal angle constraints depends upon the relative positions of the interceptor and target at the time of launch. Therefore, the limited portion is a function of the particular steering doctrine employed by the interceptor. The remaining parts of this section will examine the regions of a LAR diagram that are limited by prelaunch gimbal angle constraints for four typical interceptor steering doctrines. It will be noted from the following discussion that these prelaunch gimbal angle constraints tend to limit the minimum launch range boundary on a LAR diagram.

3.1 GIMBAL ANGLE GEOMETRY

Before examining how prelaunch gimbal angle constraints effect a LAR diagram it is well to define the gimbal angle or look angle. It can be seen from the geometry on Figure 3.1 that the gimbal angle is a spatial angle measured from the interceptor body axis to the interceptor-target line-of-sight (LOS). This angle may be expressed as:

$$\cos A = \cos A_V \cos A_S \qquad (3.1)$$

where

A = Spatial gimbal angle or look angle,

A_S = Horizontal component of gimbal angle,

A_V = Vertical component of gimbal angle.

INTERCEPTOR GIMBAL ANGLE GEOMETRY

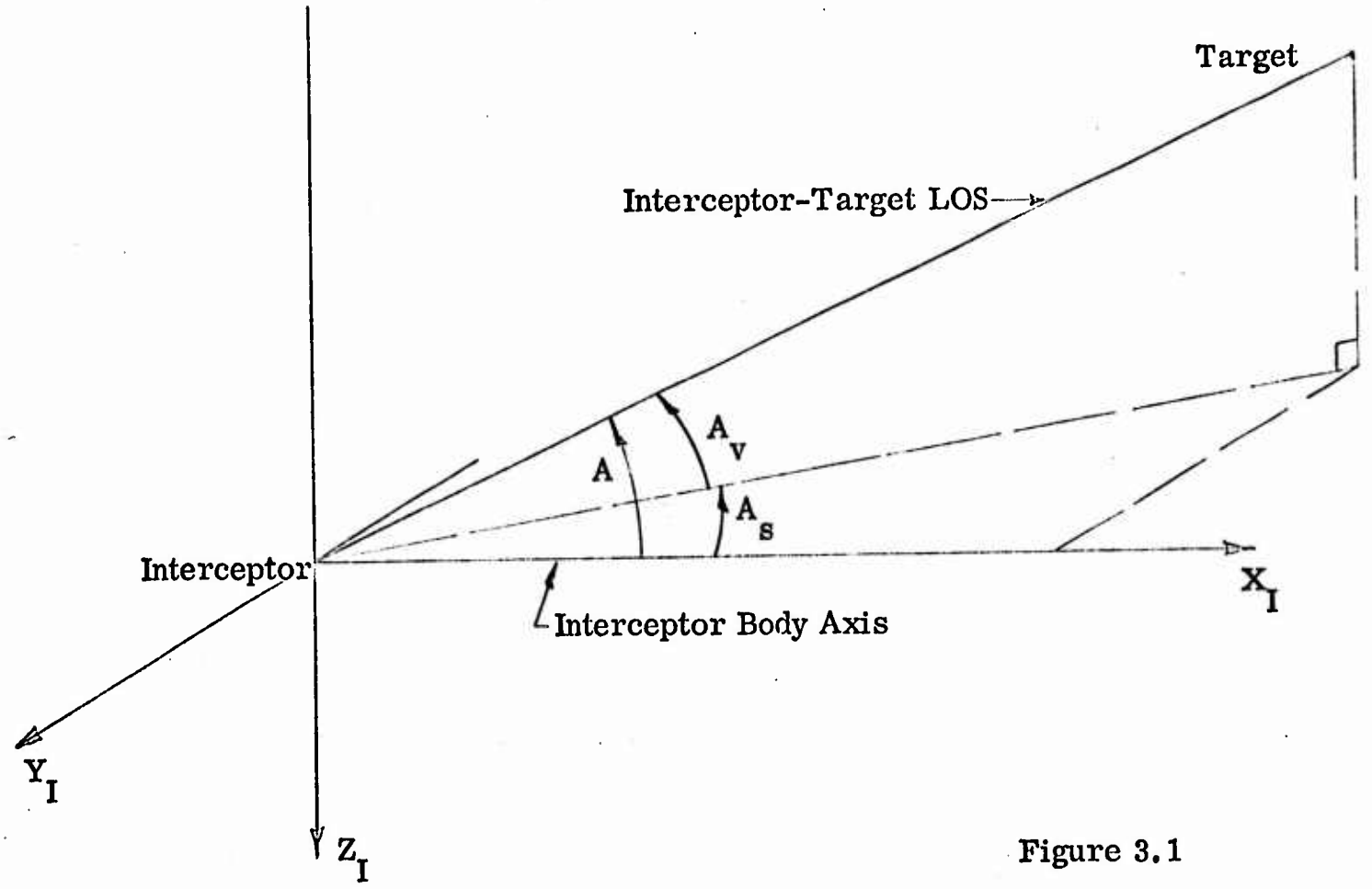

Figure 3.1

3.2 GIMBAL ANGLE CONSTRAINTS FOR PURSUIT STEERING

A pursuit steering doctrine is one in which the interceptor's velocity vector is always pointed toward the instantaneous target position. It can be seen from Figure 3.2a that, as defined here, this doctrine applies only to the horizontal plane, with the interceptor in level flight.

Since the interceptor is always pointed toward the instantaneous position of the target (in the horizontal plane) none of the LAR diagram will be limited because of horizontal gimbal angle constraints. However, in general, the interceptor and target will not be at the same altitude, and a portion of the LAR will be limited because of vertical gimbal angle constraints. The vertical look angle or gimbal angle from the interceptor to the target is given by:

$$A_v = \sin^{-1} \frac{\Delta_h}{R_{IT}} \qquad (3.2)$$

INTERCEPTOR STEERING DOCTRINES

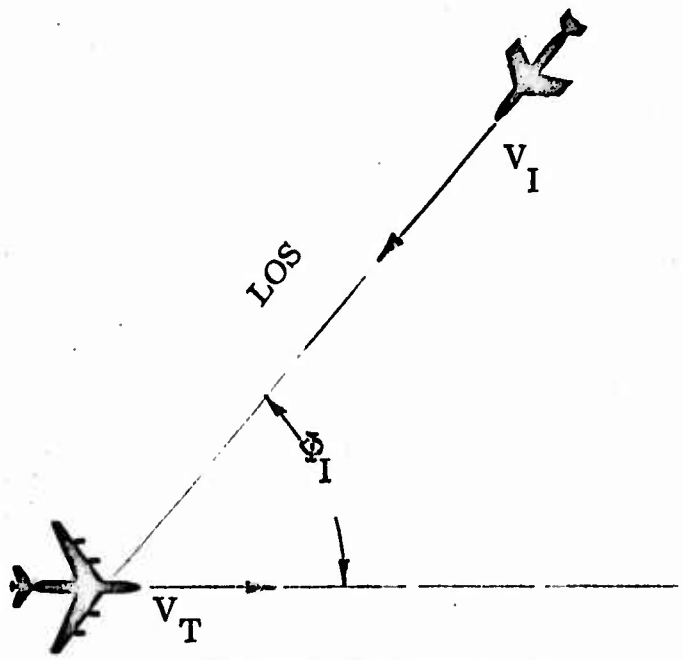

Pursuit Steering (a)

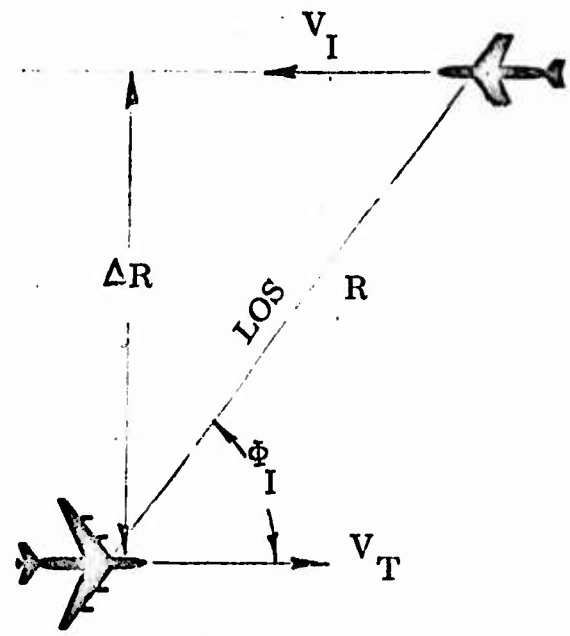

Parallel Offset Steering (b)

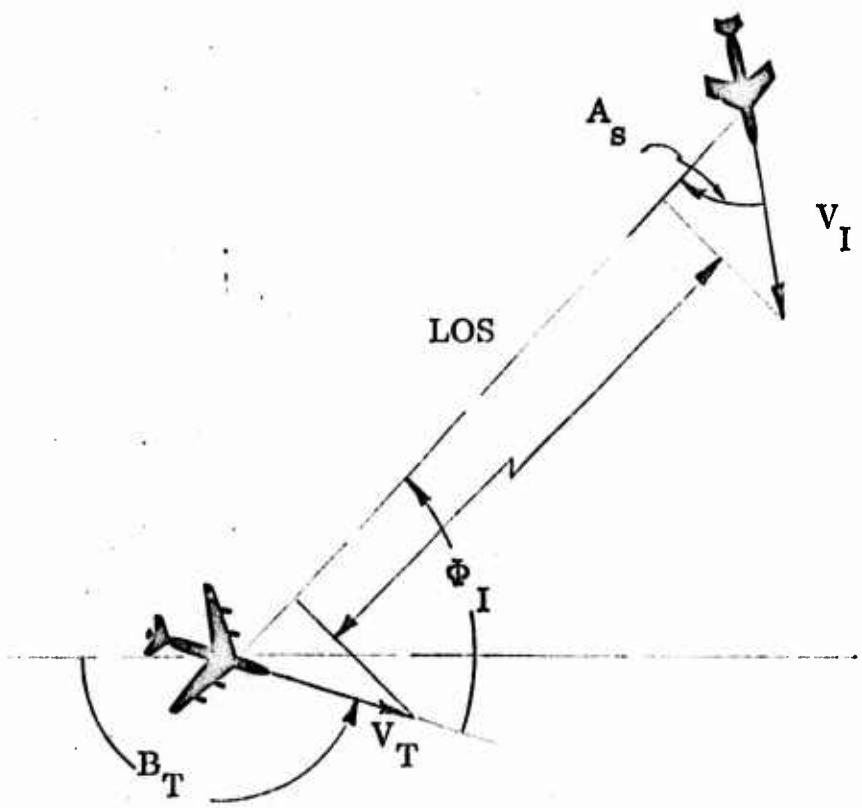

Interceptor Collision Steering (c)

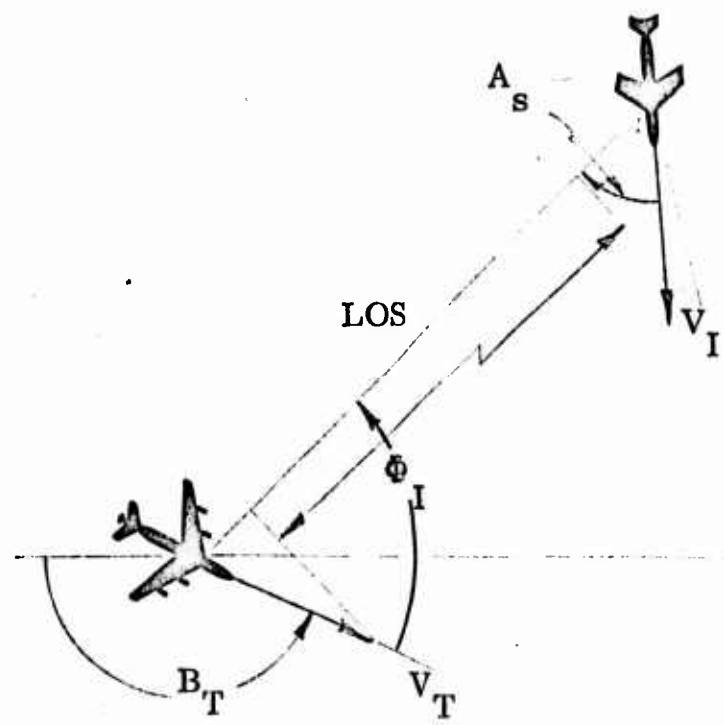

Missile Collision Steering (d)

Figure 3.2

where

A_v = Vertical component of the gimbal angle,

Δh = Interceptor to target altitude differential,

R_{IT} = Interceptor to target range.

The region excluded from the potential LAR by vertical gimbal angle limits will be a set of cones with their axis along a vertical line through the target and with a half angle equal to the compliment of the "pertinent" vertical gimbal angle limit. This is illustrated in Figure 3.3a. The "pertinent" vertical gimbal angle limit is the smaller of the gimbal limits of either the interceptor or missile. It should be mentioned here when the missile's vertical gimbal limits are the constraining factor, the half angle of the cone is usually increased (more LAR is excluded) to account for missile perturbations caused by the flow field around the interceptor.

3.3 GIMBAL ANGLE CONSTRAINTS FOR PARALLEL OFFSET STEERING

In parallel offset steering the interceptor velocity vector is aligned parallel to the target velocity vector. The interceptor and target may be flying in opposing directions, as illustrated in Figure 3.2b; or the interceptor may be flying in the same direction as the target.

A portion of the LAR will be limited because of both horizontal and vertical gimbal angle limits when parallel offset steering is employed by the interceptor. The vertical exclusion region, in this case, is the same exclusion region as it was for pursuit steering. Again the vertical exclusion region is the result of an altitude differential between the interceptor and target. Since,in general, the interceptor will not be pointing directly at the target for parallel offset steering, the horizontal gimbal limits will also act to exclude some area from the LAR. The horizontal component of the gimbal angle is given by:

$$A_s = \sin^{-1} \frac{\Delta R_o}{R_{IT}} \qquad (3.3)$$

where

A_s = Horizontal component of the gimbal angle,

ΔR_o = Interceptor-to-target horizontal offset,

R_{IT} = Interceptor-to-target range.

veda INCORPORATED

EFFECT OF GIMBAL LIMITS ON LAUNCH ACCEPTABILITY REGIONS FOR VARIOUS STEERING DOCTRINES

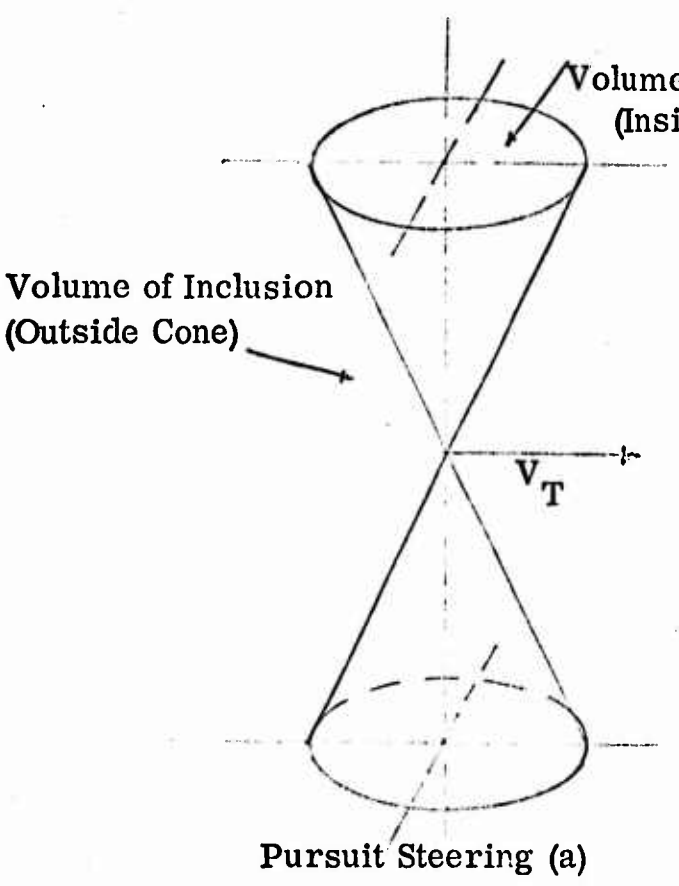

Pursuit Steering (a)

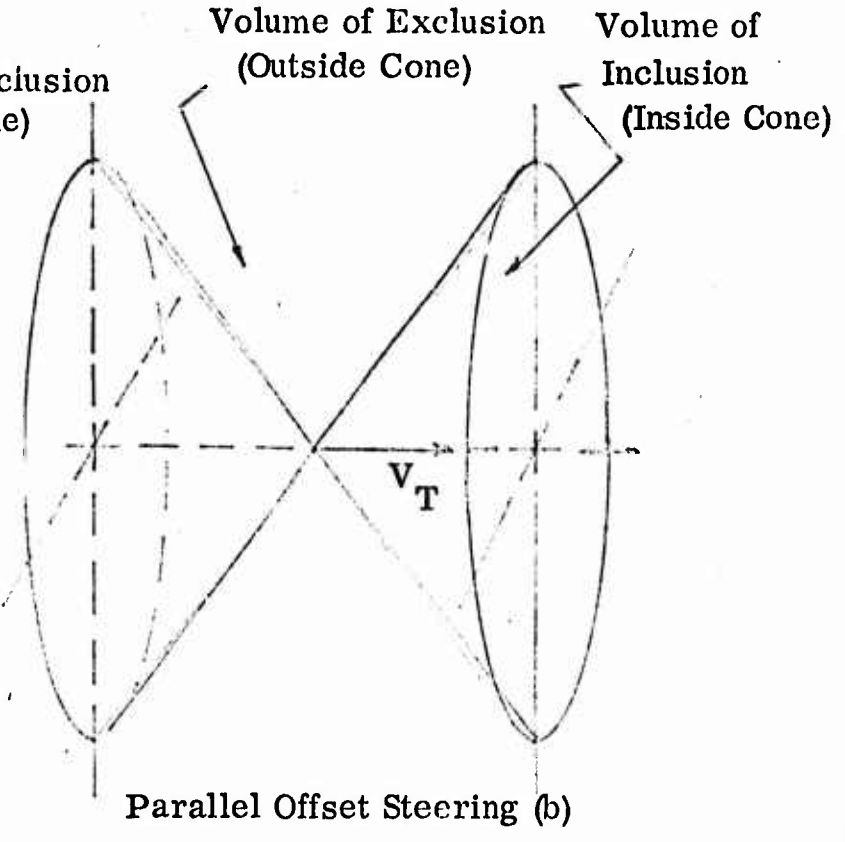

Parallel Offset Steering (b)

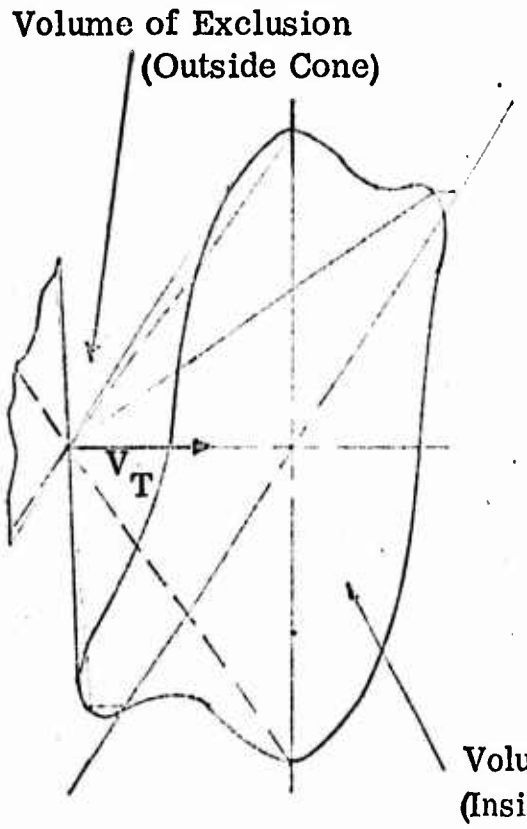

Interceptor Collision Steering (c)

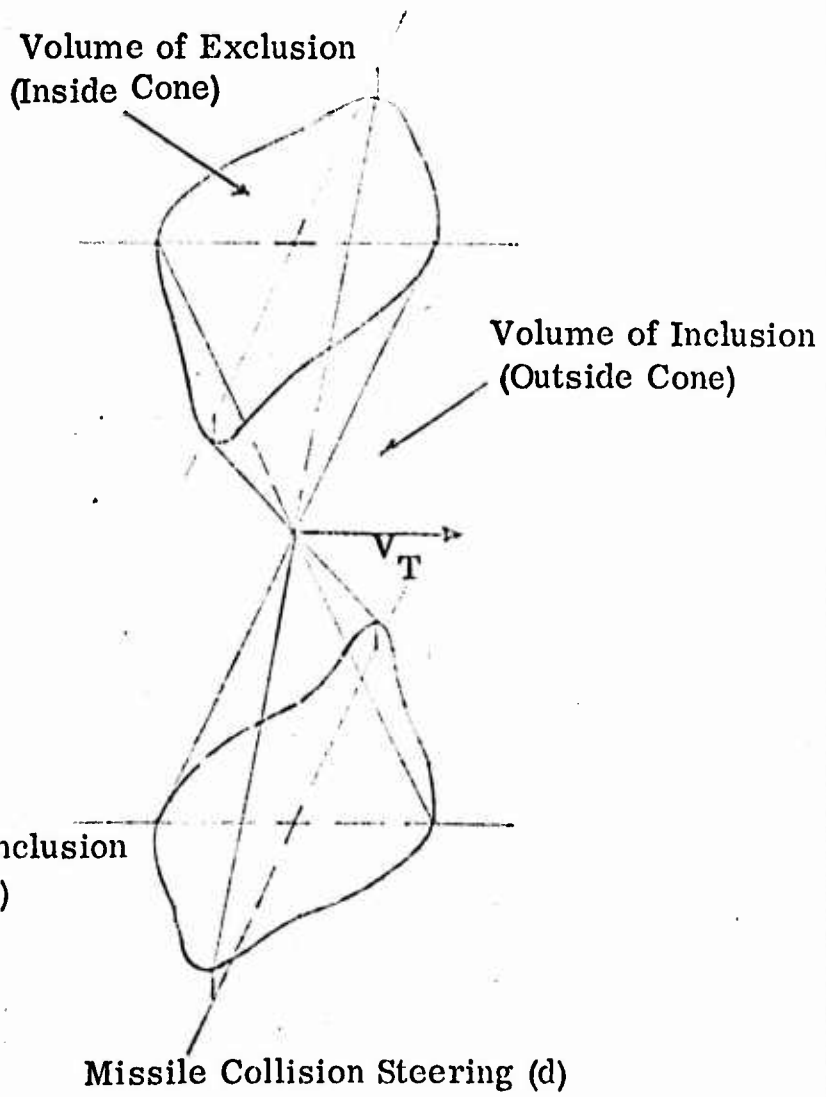

Missile Collision Steering (d)

Figure 3.3

The region limited from the potential LAR by gimbal constraints may be visualized by first assuming the interceptor and target are flying at the same altitude. The included area will now be a pie-shaped wedge on the horizontal plane. This wedge will either be in front of or behind the target (depending whether the interceptor is flying in the opposite direction or the same as the target. If the interceptor is allowed to change altitude now, vertical gimbal limits come into play. The total limited region is illustrated in Figure 3.3b. It is a disk with a wedge shaped cross-section. The axis of the disk lies in the direction of the target velocity vector. Again the "pertenent" half-angles of the cone will be determined by the smaller of either the interceptors or the missile's horizontal and vertical gimbal angles.

3.4 GIMBAL ANGLE CONSTRAINTS FOR INTERCEPTOR COLLISION STEERING

Interceptor collision steering as illustrated in Figure 3.2c denotes a steering doctrine in which the interceptor and target are on a collision course, in the horizontal plane. In general an actual collision will not occur, because the interceptor and target are not flying at the same altitude.

Since the course the interceptor flies is a function of the:

1. Target velocity,
2. Interceptor velocity,
3. Interceptor-to-target aspect angle,
4. Interceptor-to-target altitude differential,

the region limited from the potential LAR will also be a function of these factors. The first three of these factors determine the horizontal interceptor-to-target gimbal angle, while the last determines the vertical gimbal angle.

The limited region due to vertical gimbal angle limits is the same in this case as for the two previous cases. Namely, a set of inverted cones with their centers at the target.

The region limited because of horizontal gimbal limits may be determined by considering the geometry in Figure 3.2c. In order to insure a collision the components of interceptor and target velocities normal to the LOS must be equal. Therefore:

$$V_I \sin A_s = V_T \sin (\pi - B_T + \Phi_I) \qquad (3.4)$$

transposing this equation we find the horizontal projection of the gimbal angle is given by:

veda INCORPORATED

$$A_s = \sin^{-1} \frac{V_T}{V_I} \sin (\pi - B_T + \Phi_I) \qquad (3.5)$$

The total gimbal angle given by equation 3.1 will be somewhat larger for interceptor collision steering than for pursuit or parallel offset steering. Thus, the region excluded from the potential launch acceptability region, in this case, is larger. Although the excluded region could take many shapes for this type of steering doctrine a quali tative idea of what it might look like is given in Figure 3.3c.

It should be mentioned that for some values of interceptor and target velocities and interceptor-to-target aspect angle it may not be possible to fly a collision course and still remain within the gimbal limits of either the missile or the interceptor. For these cases the interceptor will fly at the largest possible lead angle where it can still maintain track on the target. If this occurs, then the region limited by gimbal constraints will appear as Figure 3.3d.

3.5 GIMBAL ANGLE CONSTRAINTS FOR MISSILE COLLISION STEERING

Missile collision steering is, in many respects, similar to interceptor collision steering. In this case, however, the interceptor solves the intercept triangle (equation 3.4) by assuming an average speed which is equal to the average missile speed.

The gimbal angle constraints for missile collision steering are a function of the same factors as for interceptor collision steering; except that the interceptor velocity V_I is replaced by the average missile velocity V_{MA}, in equation 3.5. In general, the lead angle for missile collision steering will be "inside" or smaller than that for interceptor collision steering. This is because the average missile velocity is usually higher than the interceptor velocity. The lead angle is indicated in Figure 3.2d, note that it is "inside" the angle necessary to keep the LOS from rotating.

As for interceptor collision, the volume limited by gimbal angle constraints may take on many shapes. However, it will lie somewhere between the volumes which are limited for pursuit steering and interceptor collision steering. A qualitative idea of what it might look like is illustrated in Figure 3.3d.

SECTION 4.0

POST LAUNCH AERODYNAMIC CONSTRAINTS

This Section presents a qualitative discussion of the post launch aerodynamic constraints on the missile. These constraints and factors tend to limit both the maximum and minimum launch range of the missile.

4.1 MAXIMUM AERODYNAMIC RANGE

One of the primary objectives of a long range air-to-air guided missile is to obtain optimum performance and the longest launch range over the maximum spread of anticipated target altitudes and velocities. There are, of course, many factors which influence the performance and launch range of an air-to-air missile. Some of these are:

1. Target Altitude and Velocity,
2. Launch Altitude and Velocity,
3. Missile Propulsion Characteristics,
4. Trajectory Shape,
5. Missile Maneuver Capability, and
6. Missile Drag Characteristics.

4.1.1 Attack Condition

A LAR diagram is defined by an attack condition. The speed and altitude of the target as well as the speed and altitude of the interceptor at launch establish the attack condition.

It can generally be said that increases in the speed and altitude of either the interceptor or target act to increase the aerodynamic launch range of a missile. These effects are illustrated in Figure 4.1 where a typical maximum aerodynamic LAR boundary is shown as a function of the speed and altitude of the target for two interceptor speeds.

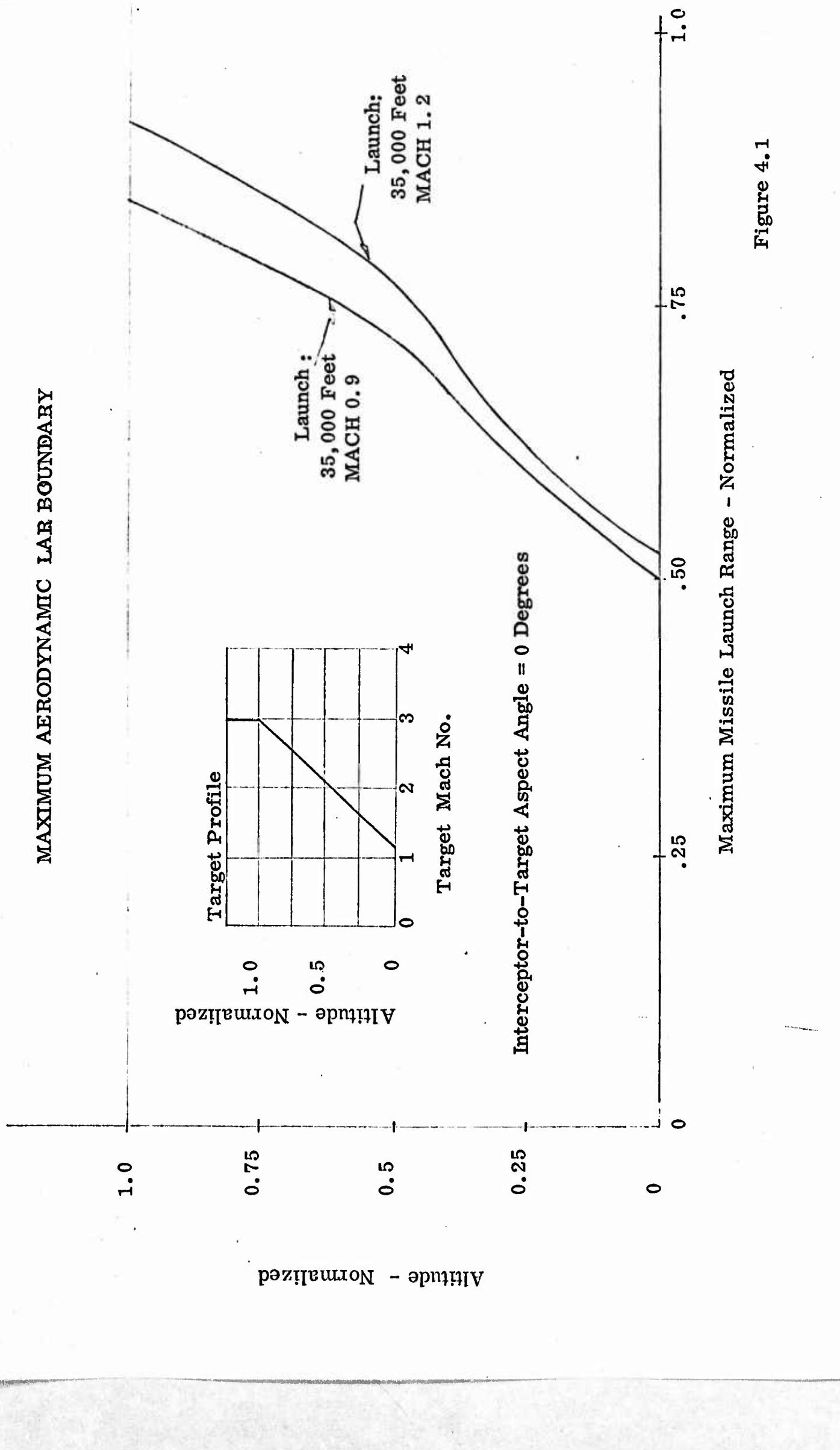
MAXIMUM AERODYNAMIC LAR BOUNDARY
Launch:
35,000 Feet
MACH 1.2
Launch:
35,000 Feet
MACH 0.9
Target Profile
Altitude - Normalized
1.0
0.5
0
0
1
2
3
4
Target Mach No.
Interceptor-to-Target Aspect Angle = 0 Degrees
Altitude - Normalized
1.0
0.75
0.5
0.25
0
0
.25
.50
.75
1.0
Maximum Missile Launch Range - Normalized

Figure 4.1

The fact that increasing target velocity acts to increase the maximum aerodynamic launch range of a missile is easily understood by considering that a faster target flies further during a given missile flight time. The most important fact to be gleaned from the Figure though, is the effect of target altitude on the maximum aerodynamic range of the missile.

Figure 4.1 shows a marked decrease in aerodynamic launch range with decreasing target altitude. This clearly illustrates the effect that zero lift drag has on the missile's performance. As the altitude of the target decreases, the missile also is forced to fly at lower altitudes. The increased air density creates high dynamic pressure on the missile and available trajectory energy is depleted through drag. Therefore, the missile cannot fly as far at lower altitudes on the same amount of energy as it can at higher altitudes.

4.1.2 Trajectory Shape

As mentioned previously one of the primary objectives of a long range air-to-air guided missile is to obtain optimum performance and the longest launch range over the largest spread of anticipated target altitudes and velocities.

Achieving long range and optimum performance with an air-to-air missile usually means that careful trajectory shaping be established. Trajectory shaping is one of the strongest tools presently available for controlling the aerodynamic range of a missile. The shaping process can be implemented in either of two ways. Namely, through modification of the navigation equation or by the introduction of steering biases (g-biases) into the guidance loop.

To understand the trajectory shaping process, consider a missile that is mechanized to maneuver according to the following relationship during the midcourse phase of its flight:

$$N_{cv} = K W_v + g \text{ bias} \qquad (4.1)$$

where

N_{cv} = Vertical plane commanded acceleration,

K = Guidance or navigation gain, and

W_v = Vertical plane component of the missile-to-target LOS rotation rate.

It should be noted that the basic guidance law is proportional navigation (as discussed in Section 2.3.1). In this case it is termed a "biased proportional navigation law" because of the addition of the g-bias. It is apparent from the equation that, since the bias term is an acceleration that is added to the acceleration commanded by the navigation law, the principle effect of g-bias is to cause the missile to fly higher than it would if it was commanded only by the navigation equation (note g-bias acts in the vertical plane). Figure 4.2 illustrates typical vertical plane projections of the trajectories that would result if Equation 4.1 was mechanized in an air-to-air missile. Before analyzing these trajectories we must first note that the aerodynamic drag of a supersonic missile generally consists of three types:

1. Wave drag,

2. Skin friction, and

3. Drag due to normal force (induced drag).

The total of the wave drag (the drag forces due to pressures acting on the missile at zero angle of attack) and the skin friction is usually referred to as the zero-lift drag. Whereas, the component of normal force acting in the airstream direction (and existing solely because of the resultant normal force) is referred to as induced drag. Large penalties of induced drag may occur when the missile is required to maneuver (exert normal force). This is why it is desirable to expect long range guided missiles to perform the major portion of their flights under conditions of low maneuverability and then to "pull" large maneuvers during the terminal phase.[2]

Consider, now, trajectory "a" on Figure 4.2. Here the g-bias term in Equation 4.1 is zero, and it is easily seen that at no time during its flight does the missile rise above the altitude it was launched from (except, of course, during the final intercept portion of the trajectory). The reason the trajectory exhibits this behavior is easily understood when we note the effect of gravity. Since the rotation rate of the missile target line-of-sight is low during the early phase of the missile's flight (this is especially true for long range launches) the accelerations commanded by Equation 4.1 are also small. Therefore in the absence of the bias term, the missile is unable to adequately offset the downward acceleration of gravity. The result is that the missile is forced to a lower altitude. As the range from the missile to the target decreases the line-of-sight rate increases, thereby causing larger guidance commands and enabling the missile to accelerate upward and raise its trajectory. It should also be noted that the phenomenon described above is accentuated for those cases where the interceptor launches the missile by giving it an initial downward acceleration. It is obvious that this type of trajectory is not desirable since much of the trajectory energy is wasted (through induced drag) by

EFFECT OF MIDCOURSE G-BIAS

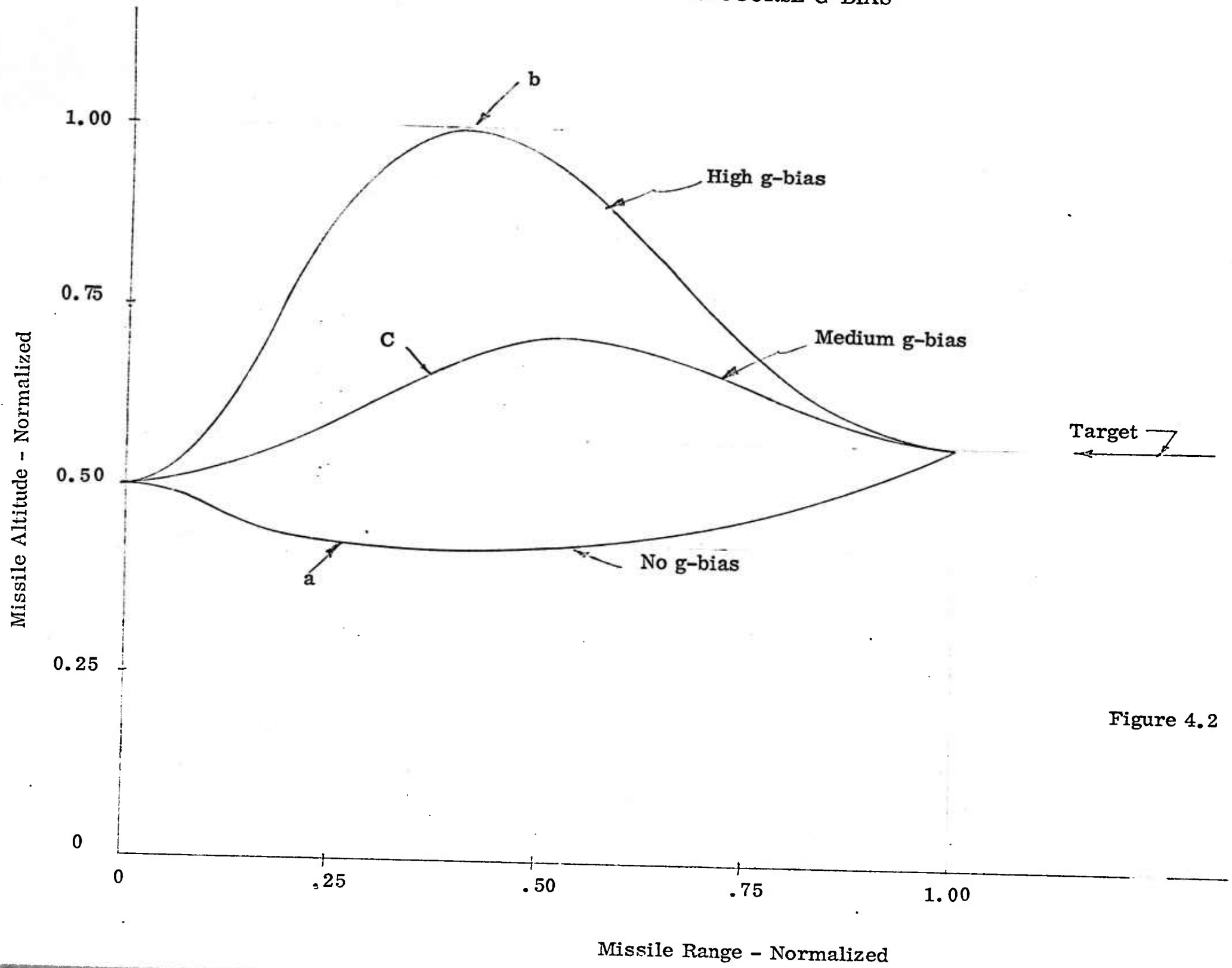

Figure 4.2

correcting for the initial drop in altitude late in the flight. This type of trajectory leads to comparatively small maximum launch ranges and is not desirable for attacks where the target is above the interceptor.

Next, consider trajectory "b" on Figure 4.2. This is an example of a trajectory that would result if a very large value of a g-bias (approximately 3 to 8 g's) was employed in the guidance equation. Here the bias term dominates early in the trajectory when the missile-target line-of-sight rate is small. As a result, the missile is forced to a rather high altitude, and follows an inefficient, lopsided trajectory. The trajectory is inefficient because much of the available trajectory energy is wasted through induced drag and by the missile climbing to altitude. Also if the value of g-bias is too large the missile will be forced to climb to an altitude where the air density is too low to ensure stable missile flight.

At this point we are now able to see that the trajectory shaping process consists of trading off the apogee of the trajectory against the magnitude of the g-bias and the subsequent increase in drag associated with it. However, it is evident from trajectory "a" on Figure 4.2 that it is desirable to select a g-bias that causes the missile to fly above the path normally commanded by the guidance system. Marked gains in maximum launch range can be obtained by flying at higher altitudes where the reduction in zero lift drag (due to lower dynamic pressure) offsets the increase in induced drag that results from large maneuver requirements and larger angles of attack.

The result of a trajectory shaping process to determine the "best" g-bias would produce a trajectory similar to trajectory "c" in Figure 4.2. Here better use is made of the available trajectory energy by the choice of a medium level g-bias. Since the g-bias is not as large as in the previous case the missile is not penalized by large amounts of induced drag and it is able to achieve longer maximum launch ranges and higher terminal velocities with the same amount of trajectory energy as the two previous cases.

The trajectory shaping process is not finished when the optimum g-bias has been selected. It is now necessary to determine a value of mid-course navigation gain (K in Equation 4.1), consistent with the g-bias to finally provide the desired trajectory shape.

The effects of changes in navigation gain on the shape of a long range missile's trajectory are illustrated in Figure 4.3. In trajectory "a" the mid-course navigation gain is too large and the missile counters the attempt of g-bias to raise its trajectory. Since the large navigation gain acts on the missile-target line-of-sight rate to produce large missile maneuvers, much of the available trajectory energy is again wasted by induced drag. The result

EFFECT OF MIDCOURSE GAIN

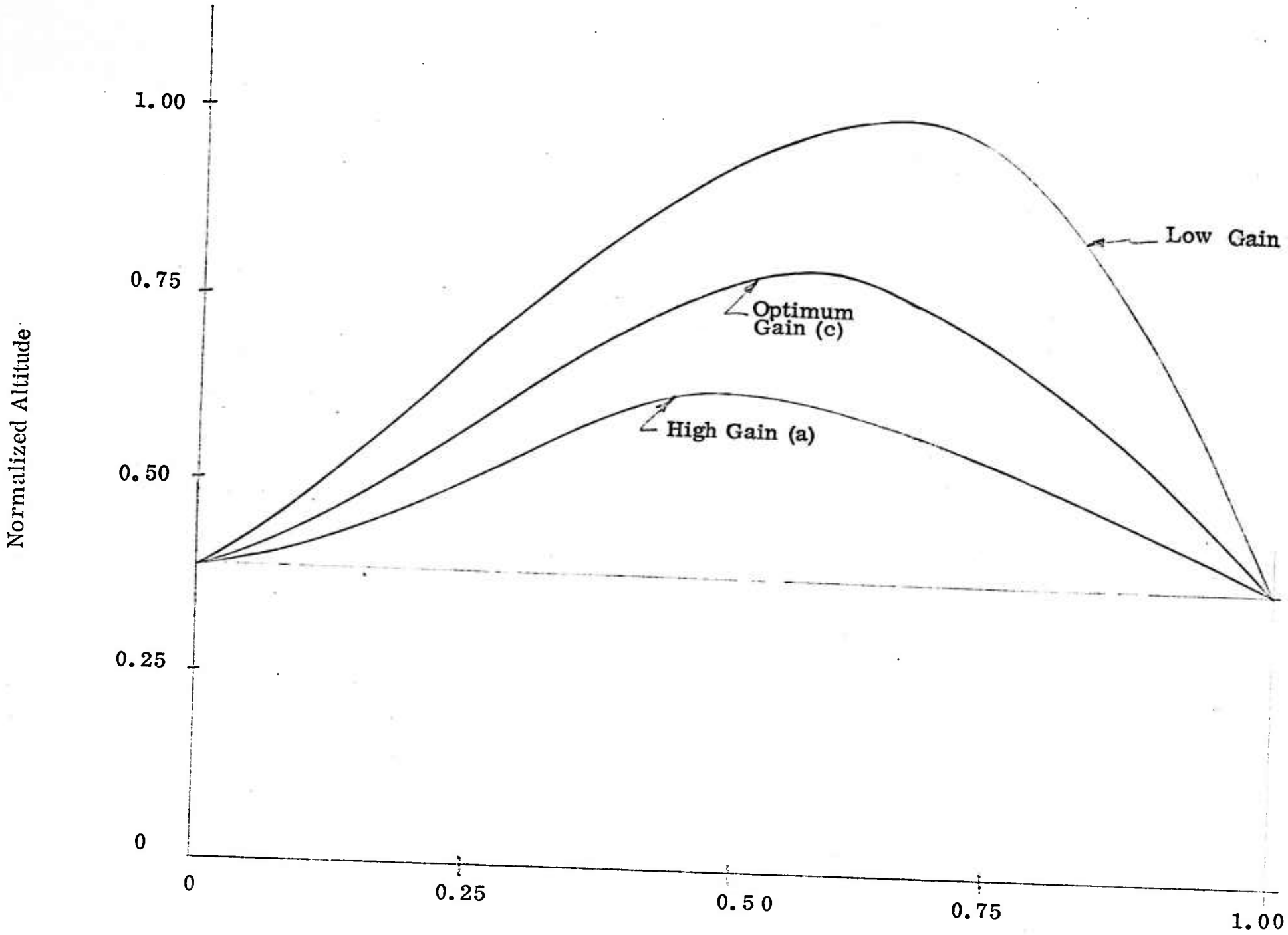

Figure 4.3

is that the missile flies a "flatter" trajectory. Large values of navigation gain may also, in some instances, act to reduce the maximum launch range of the missile.

Trajectory "b" represents a typical trajectory that results when the navigation gain is too low. Here the missile responds very little to line-of-sight rate during the first three quarters of the trajectory and the g-bias forces the missile to a high altitude. The missile only begins to respond to line-of-sight information during the latter portion of the trajectory. The result is that the missile is forced to dive to effect an intercept. When the missile is forced to dive a very good possibility exists that some of the geometric constraints (discussed in Section 5.0) may be violated and an intercept would, therefore, be impossible.

The final result of a trajectory shaping process to determine the "best" g-bias and navigation gain would produce a trajectory similar to trajectory "c" in Figure 4.3. It must be remembered, though, that the gain and g-bias that is optimum for one set of launch conditions (i.e., target speed, altitude, range and aspect angle) may not be optimum for another. Therefore an extensive trajectory analysis must be performed to adequately predict the variation of these factors with launch conditions.

4.1.3 Maximum Missile Flight Time

Another factor that tends to limit the maximum launch range of an air-to-air missile is the maximum missile flight time. This constraint is most prevalent when the missile is launched against low altitude, low speed targets, since these attacks are characterized by relatively low average missile-to-target closing rates. Maximum missile flight time also tends to limit the missile's launch range for a rear hemisphere attack, since these also are characterized by low average closing rates.

The maximum flight time of an air-to-air missile is specified by the expected life of its various power supplies and its supply of hydraulic fluid (for actuation of its control surfaces). For contemporary missiles the maximum flight time is approximately one to three minutes.

4.1.4 Missile Maneuverability

In order to understand how the maneuver capability of the missile effects its performance it is important to note that difference between two "types" of missile accelerations.

1. Command Acceleration, and

2. Achieved Acceleration.

These accelerations are, in turn, limited by the

1. Aerodynamic maneuver limit, and

2 Structural maneuver limit

of the missile.

First the commanded acceleration is the lateral maneuver commanded by the missile's navigation law. This is the N_c as discussed in Section 2.3.1 and 2.3.2, which is used to guide the missile to the target. After N_c has been determined by the missile's control system, commands are sent to the missile's aerodynamic control surfaces to produce N_A, the achieved acceleration. A single missile time constant (τ_r) is normally used for analysis purposes to account for time lags in the missile's control system and control surfaces. The missile response time (τ_r) is defined as the amount of time necessary for the achieved acceleration N_A to reach 63% of its steady state value after a step command N_c has been introduced to the closed loop control system. Note that the definition of τ_r follows the conventional definition for the response time of a first order lag. The control systems of homing missiles, however, usually take the form of a series of first order lags. Control system transfer functions typically take the form:

$$Y(S) = \frac{S}{(\tau_1 S+1)} \cdot \frac{1}{(\tau_2 S+1)} \cdot \frac{\tau_3 S-1}{(\tau_4 S-1)(\tau_s S+1)} \qquad (4.2)$$

where the τ_i represent the time constants of control elements in the tracking loop and autopilot.

The higher order representation is more realistic than the first order lag and must be used for the investigation of high frequency phenomenon involving the missile. The definition of τ_r is, therefore, arbitrary— but still valid since the overall trajectory performance of the missile during an intercept is basically a low frequency phenomenon. The response times of contemporary air-to-air missiles are on the order of 0.25 to 2.0 seconds.

There are, of course, limits on the achieved acceleration N_A. These limits are determined by the maximum load factor of the missile's structure and the aerodynamic maneuver limit. The structural limit is specified by the acceleration the missile can sustain before incurring damage to its structural members. Maximum structural load factors for contemporary missiles range from 10 to 20 -g's.

The aerodynamic maneuver limit used for the determination of aerodynamic range limitations on a LAR diagram is specified by the formula:

$$N_{ALIM} = C_{NMAX}(M)\ Q\ S \qquad (4.3)$$

where

N_{ALIM} = Aerodynamic maneuver limit,

$C_{NMAX}(M)$ = Maximum normal force coefficient as a function of missile Mach number,

Q = Dynamic pressure, and

S = Aerodynamic reference area.

The curve of C_{NMAX} vs Mach number is determined from wind tunnel data as the maximum acceleration the missile can achieve at a given Mach number for a maximum deflection of its control surface.

To summarize now: the missile receives a commanded acceleration from the guidance system and responds to yield the achieved acceleration. The commanded acceleration is limited by the control system to be less than a predetermined structural limit, and the achieved acceleration is limited by the maximum aerodynamic capability of the missile.

4.2 MISSILE AERODYNAMIC RANGE SUMMARY

The effects of all the factors discussed in this section act to produce a maximum aerodynamic launch region around the target that takes the form of an ellipse as illustrated in Figure 4.4. This elliptical region is in turn limited by various other post, launch constraints which will now be discussed.

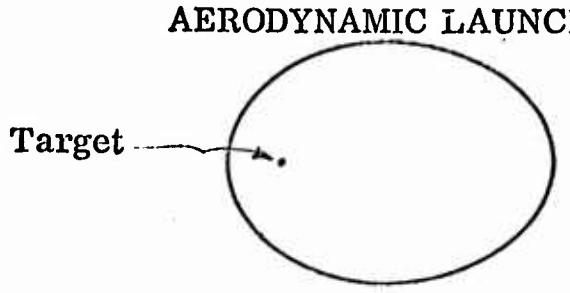

Figure 4.4

veda INCORPORATED 44

SECTION 5.0

POSTLAUNCH GEOMETRIC CONSTRAINTS

This section discusses the two basic postlaunch geometric constraints. They are:

1. Missile climb or dive angle limits, and

2. Missile seeker gimbal angle limits.

5.1 MISSILE CLIMB OR DIVE ANGLE LIMITS

The maximum climb or dive angle (attitude angle θ in Figure 5.1) is limited in some contemporary air-to-air missiles by gimbal configuration of the roll attitude gyro. As this gimbal lock is approached (by the missile assuming a large angle θ) the vertical gyro will tumble, thereby destroying the attitude reference for the missile's autopilot.

The maximum climb or dive angle limits usually tend to constrain the minimum launch range of the missile's LAR. This is especially true for medium-to-high altitude launches against low altitude targets where missile pitch attitudes sometimes approach 90 degrees near the end of flight. The climb or dive angle limits may also act to establish a lower bound on the midcourse navigation gain, since (as it will be recalled from Section 4.1.2) a low value of navigation gain allows the missile to reach a very high altitude before it dives at the target during intercept (trajectory "b" on Figure 4.2).

The maximum climb or dive angle will, of course, be different for different missile systems. However, it usually ranges between 80 and 90 degrees.

5.2 MISSILE SEEKER GIMBAL LIMITS

In order for an air-to-air missile to home on a target it must be able to "look" at that target throughout the guided portion of its flight. This, of course, is true for semi-active homing guidance systems as well as active homing guidance systems. A missile is ability to "look" at a target is governed in part by the gimbal limits on its radar seeker. This limit is termed "gimbal angle limit" or "look angle limit".

CLIMB OR DIVE ANGLE LIMITS

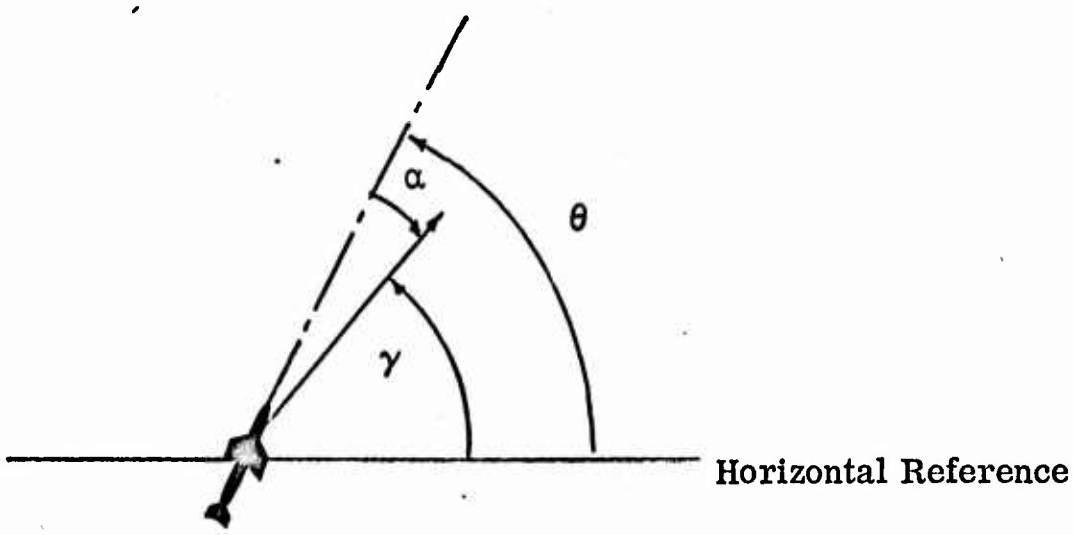

γ = Flight Path Angle

α = Angle of Attack

θ = Pitch Altitude Angle

Figure 5.1

The missile-to-LOS gimbal angle is illustrated in Figure 5.2. It can be seen from the Figure that the gimbal angle is the spatial angle measured from the missile body axis to the missile-to-target LOS. This angle is given by:

$$\cos G = \cos G_s \cos G_v \qquad (5.1)$$

where

G = Spatial gimbal angle or look angle,

G_s = Slant plane component of seeker gimbal angle, and

G_v = Vertical plane component of seeker gimbal angle.

Trajectory analysis shows that at launch and throughout a typical missile flight, as the relative positions and velocities of the missile and target change, the angle G changes also. Under certain conditions the gimbal angle may assume large values, in fact, it may be required to assume angles that are beyond the limit set by its gimbal stops. This of course, results in an aborted trajectory since the missile can no longer "look" at the target and extract guidance information from it. When this occurs the LAR diagram is said to be "gimbal

SEEKER GIMBAL ANGLE GEOMETRY

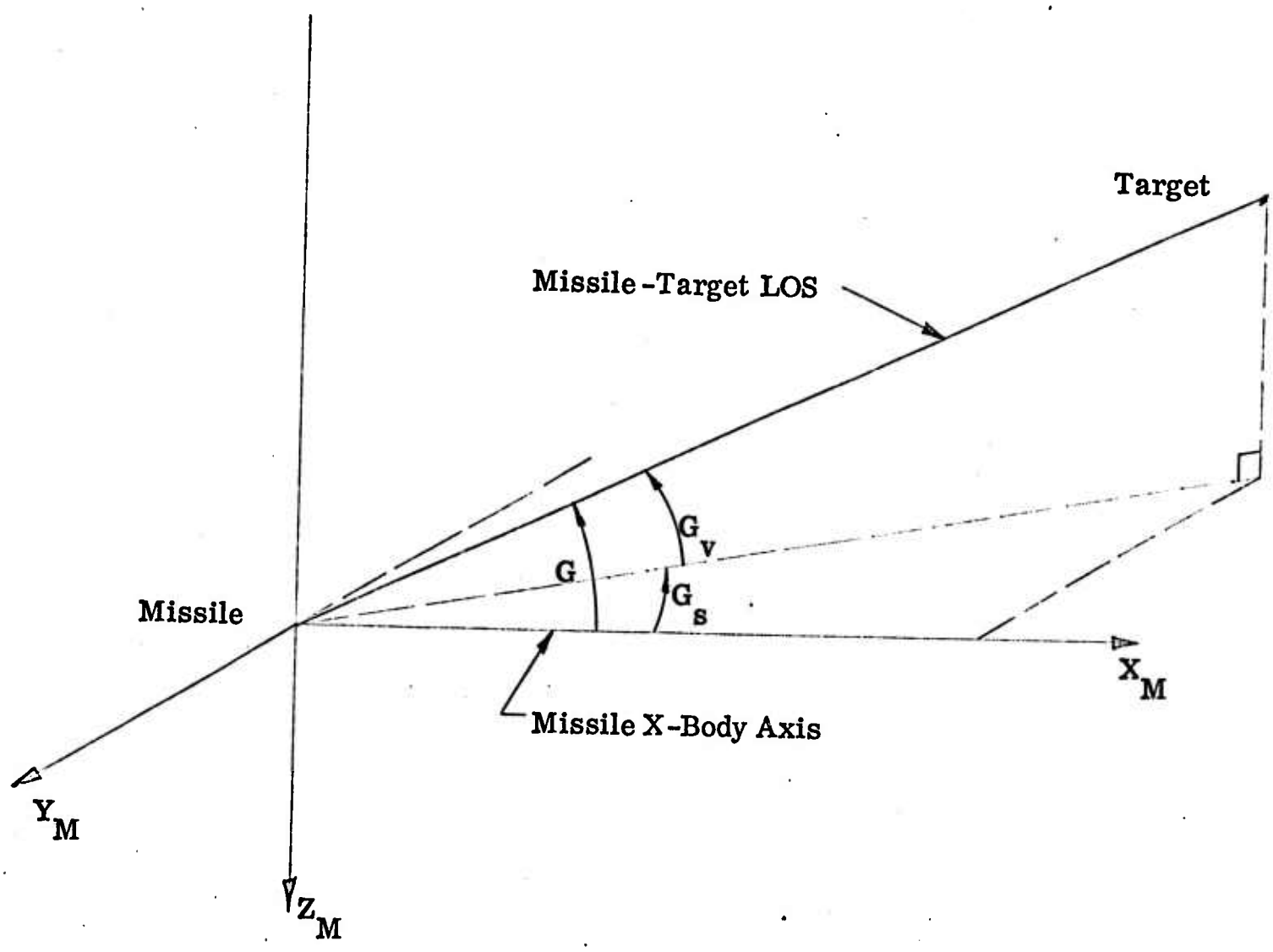

Figure 5.2

angle limited" at that particular launch condition. Extensive analysis has shown that gimbal angle limits may occur under certain predictable situations. These situations will now be discussed.

Since the missile must track the target at launch or shortly thereafter, the missile-to-LOS gimbal angle must be within its required limits during the launch and separation phase. Both the unpredictable flow field around the interceptor and switching transients caused by control system activation could cause the missile to exceed its gimbal limits during this time. For the most part, these perturbations are unpredictable so an artificial limit (less than the actual limit) is usually established on the launch gimbal angle during trajectory analysis.

The second situation in which a large gimbal angle may be required is during the trajectory when the missile has a low velocity relative to the target. This effect is most apparent for missiles that employ a proportional navigation guidance technique. Consider the guidance geometry illustrated for proportional navigation in Figure 2.2. If small angles of attack are neglected this Figure may be redrawn as Figure 5.3.

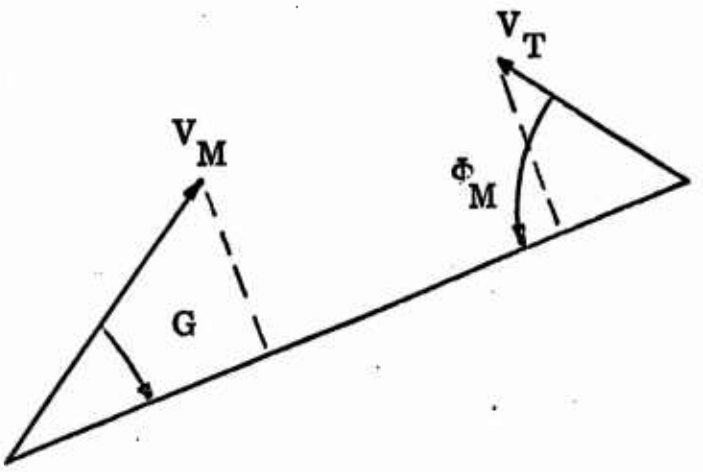

FIGURE 5.3

GUIDANCE GEOMETRY NEGLECTING ANGLES OF ATTACK

It will be recalled from Section 2.3.1 that proportional navigation attempts to keep the missile-target LOS from rotating. Therefore, from Figure 5.3 the components of missile and target velocities normal to the LOS must be equal. As the speed of the missile changes the angle G will change accordingly to keep the LOS from rotating. Very large values of V_M require only small values of G, whereas, a low missile velocity relative to the target, requires a very large gimbal angle. It is during this time that the gimbal limits may be exceeded. Gimbal angle limits caused by a low missile velocity relative to the target are especially noticeable during attacks against low altitude targets from high aspect angles. This is because the missile is forced to fly at low altitudes where high drag reduces the missile's velocity.

It must be mentioned that the overall effect of gimbal angle limits on a LAR diagram, depend to a large extent on the characteristics of the specific missile system under consideration. In general, though, it may be said that gimbal angle constraints tend to limit a LAR diagram for launches at high aspect angles.

veda INCORPORATED

SECTION 6.0

POSTLAUNCH GUIDANCE CONSTRAINTS

This section presents a qualitative discussion of the effects of postlaunch guidance constraints on LAR diagrams for radar guided air-to-air missiles. The guidance constraints are divided into three parts which deal with the interceptor, the semiactive missile guidance phase and the active missile guidance phase. Since most contemporary AI radars and missile seekers employ doppler tracking filters to improve the signal-to-noise ratio of the target return, this section includes the clutter spectra and target doppler frequency behavior in the dynamic geometry of an air-to-air intercept. The clutter spectras as observed in the:

1. AI radar during the semiactive phase of a missile's flight.
2. Semiactive phase missile seeker.
3. Active phase missile seeker

are discussed in each of the three sections. Mathematical inequalities are also developed that represent the observed target doppler in each of the three clutter spectras.

In addition to analyzing the clutter problem, the effect of the midcourse navigation law on a LAR diagram is also illustrated. Finally, the terminal phase eclipsing problem and its affect on final missile-target miss distance is discussed.

6.1 INTERCEPTOR CLUTTER SPECTRA

Before examining the radar clutter spectra observed by an interceptor when it is illuminating a target, it is well to review the doppler effect.

The frequency of a signal transmitted by a moving transmitter is shifted from the stationary transmission frequency by an amount proportional to the speed of the transmitter in the direction of propagation. Consider two wave fronts emanating from a moving transmitter. The distance between the wave fronts or wavelength is changed from the stationary transmission wavelength due to the motion of the transmitter during the signal period. Thus, the actual wavelength is

$$\lambda' = \lambda \mp \frac{V \cos \Phi}{f} \qquad (6.1)$$

where

λ = the stationary transmission wavelength,

V = the speed of the transmitter,

Φ = the angle between the direction of propagation and the direction of motion of the transmitter, and

f = the stationary frequency (its reciprocal is the signal period).

Since the doppler shifted frequency must satisfy

$$f' \lambda' = f \lambda = c \tag{6.2}$$

where c is the speed of propagation, then the observed transmission frequency is

$$f' = \frac{c}{\lambda - \frac{V \cos \Phi}{f}} \tag{6.3}$$

and

$$f' = f \frac{c}{c - V \cos \Phi} \tag{6.4}$$

The shift in frequency or the doppler frequency is given by

$$f_d = f' - f = f \left[\frac{c}{c - V \cos \Phi} - 1 \right] \tag{6.5}$$

and

$$f_d = f \frac{V \cos \Phi}{c - V \cos \Phi} \tag{6.6}$$

In the case where $V << c$ Equation 6.6 becomes simply

$$f_d = \frac{V \cos \Phi}{\lambda} \tag{6.7}$$

The frequency f_d is the shift in frequency that would be observed by a stationary observer from a transmitter in motion. Because of the well known reciprocity theorem, Equation 6.7 also describes the shift in frequency observed by a moving observer from a stationary transmitter. Provided, of course, the observer is in motion relative to the propagation direction by the same $V\cos\Phi$, since the change in observed wavelength would also be defined by Equation 6.1.

If both the transmitter and observer are in motion by the speeds V_R and V_O respectively, it can be shown that the doppler shift is given by:

$$f_d = \frac{V_R \cos\psi_R + V_o \cos \Phi_R}{\lambda} \qquad (6.8)$$

Where ψ_R and Φ_R are illustrated in Figure 6.1

OBSERVER-TRANSMITTER GEOMETRY

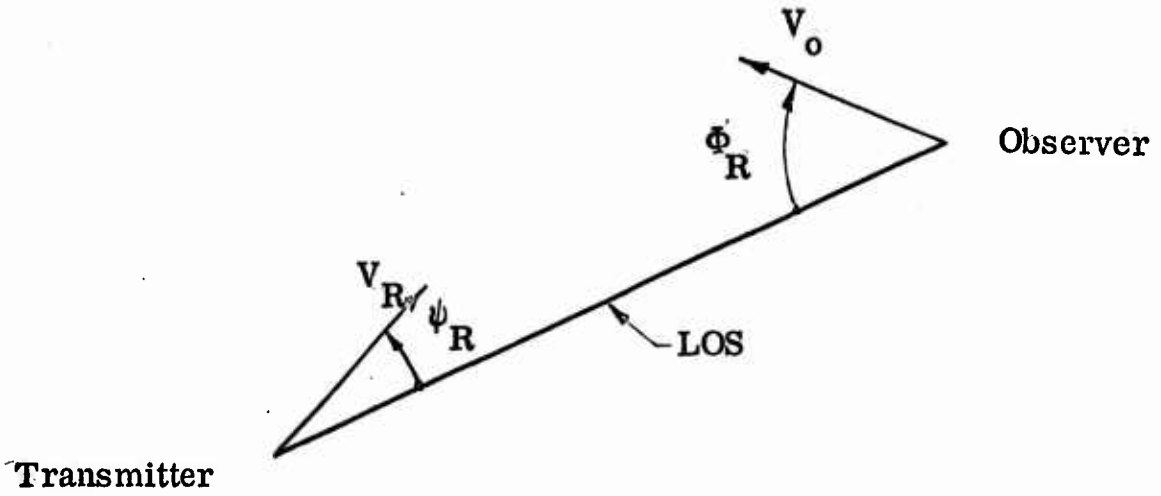

FIGURE 6.1

Equation 6.8 describes the shift in frequency that would be observed by a moving observer from a moving transmitter.

In the case where the receiver is a moving scatterer (such as a radar target) and the signal is reflected back to the radiator from which it was transmitted, the total doppler shift is simply twice that of Equation 6.8. Or:

$$f_{d_I} = \frac{2\,V_I \cos\psi_I + 2\,V_T \cos \Phi_I}{\lambda} \qquad (6.9)$$

Where

f_{d_I} = Total doppler shift of signal reflected by a radar scatterer

V_I = Velocity of interceptor

ψ_I = Spatial angle between interceptor velocity vector and interceptor target LOS

V_T = Velocity of target

Φ_I = Spatial angle between target velocity vector and interceptor-target LOS (Note: the horizontal projection of this angle is the aspect angle)

Since

$$\dot{R}_{IT} = -V_I \cos \psi_I - V_T \cos \Phi_I \qquad (6.10)$$

Where

$\dot{R}_{IT}$ = Interceptor to-target closing rate

Combining Equations 6.9 and 6.10 we have:

$$f_{d_I} = -2 \frac{\dot{R}_{IT}}{\lambda} \qquad (6.11)$$

Return now to the problem at hand, namely that of examining the radar clutter spectra observed by an interceptor when it is illuminating a target. Radar clutter has been defined as a conglomeration of unwanted radar echoes.[3] The name has been well chosen since it is descriptive of the fact that such echoes "clutter" the radar display and make the recognition of wanted echo signals difficult. Clutter return in an airborne radar is the result of signal scattering from the terrain. The sources of clutter signals are illustrated in Figure 6.2a.

The dopper frequency resulting from scattering from a given point on the terrain is given by twice Equation 6.7. (Here it has been assumed that the average speed of the terrain is zero - this may not be exactly true over sea surfaces). Since the total clutter is derived from all parts of the terrain illuminated, the clutter bandwidth is more significant than any given point (except for those particular areas noted below.) The clutter bandwidth is determined by considering all values of ψ_I between $+\pi$ and $-\pi$ (i.e. all the terrain between the rear and forward horizons for horizontal velocities, V_I).

veda INCORPORATED

INTERCEPTOR CLUTTER GEOMETRY

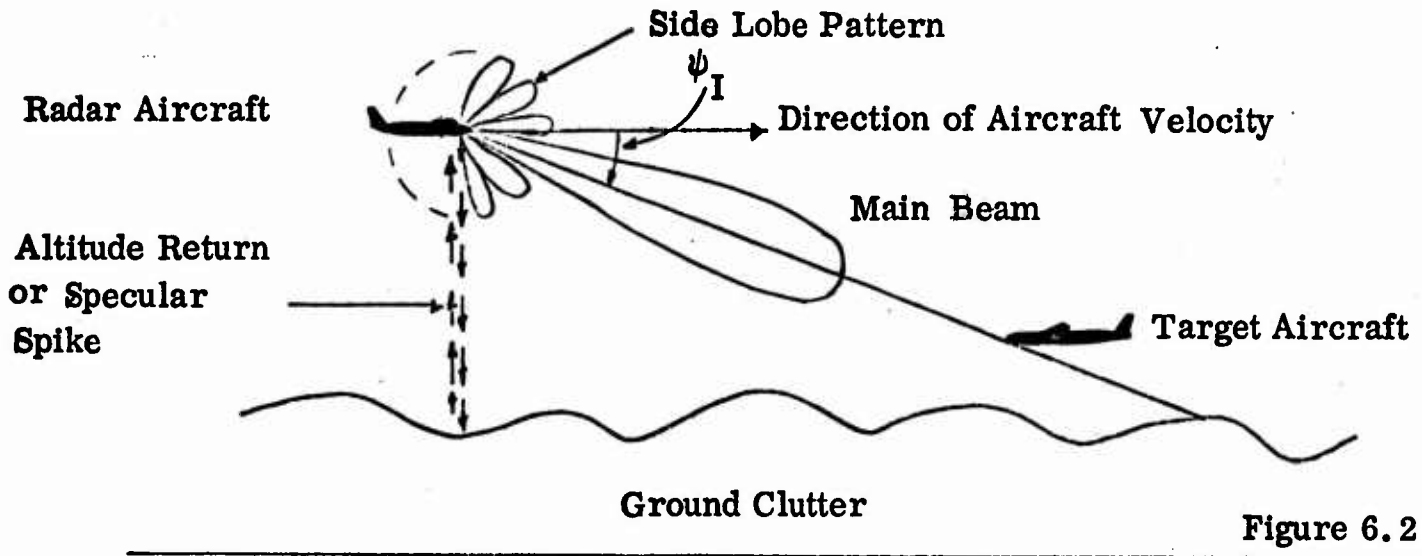

Figure 6.2 a

INTERCEPTOR RECEIVED SIGNAL SPECTRUM

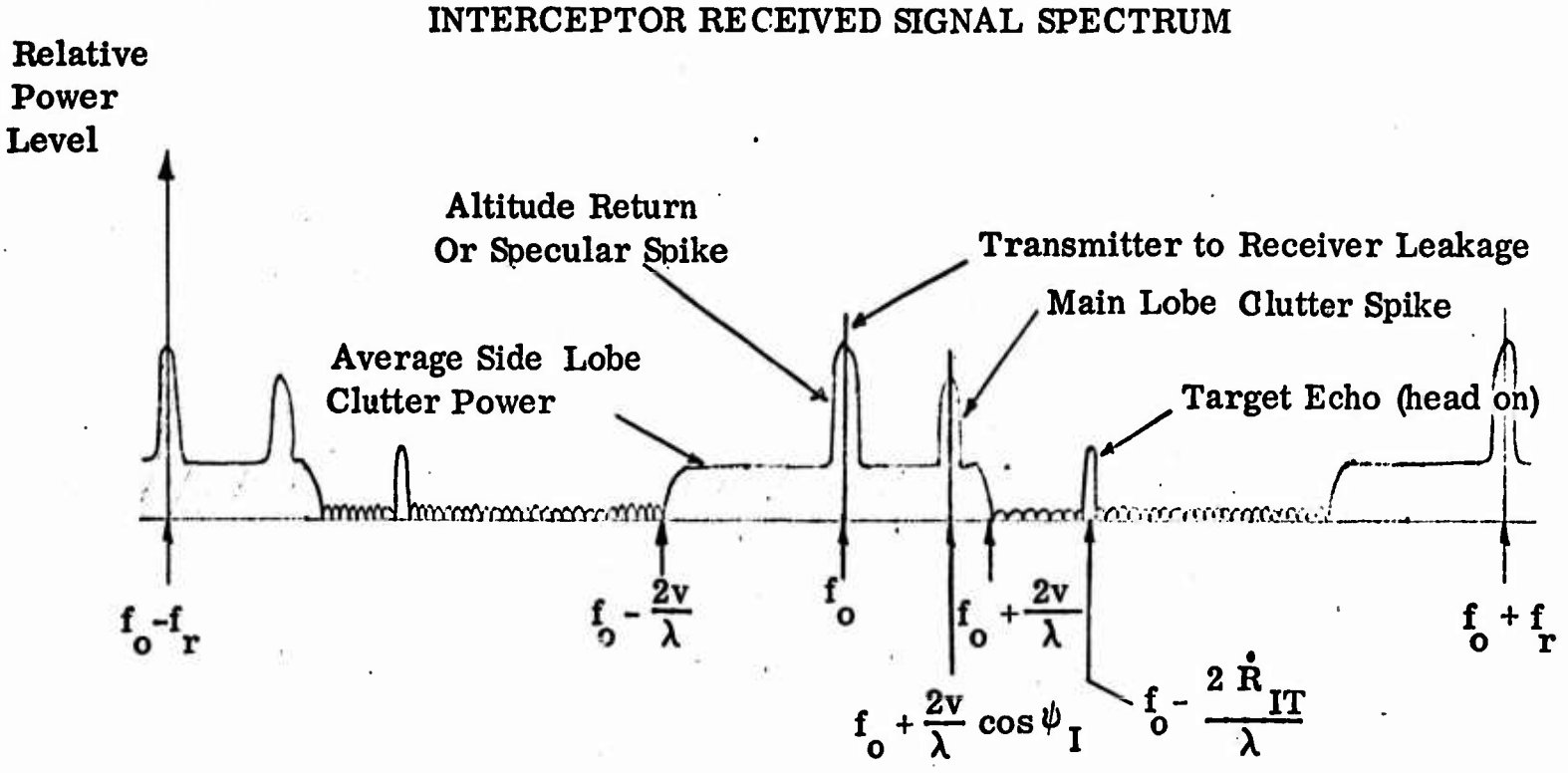

Figure 6.2 b

The clutter bandwidth (or spectrum of received signals) for a pulse modulated airborne radar are those frequencies, f, which satisfy

$$f_o - \frac{2 V_I}{\lambda} \leq f \leq f_o + 2 \frac{V_I}{\lambda} . \qquad (6.12)$$

A typical spectrum of the received signal is illustrated in Figure 6.2 b.

Only that portion of the spectrum in the vicinity of f_o is shown. The shape of the clutter spectrum about each of the other spectral components spaced at intervals equal to the pulse repetition frequency is the same as that about f_o. The leakage of the transmitter signal into the receiver produces the spike at a frequency f_o and the spikes at $f_o \pm nf_r$, where n is an integer and f_r is the pulse repetition frequency. The echo from the ground directly beneath the aircraft is called the altitude return or the specular spike. The altitude return is not shifted in frequency since the relative velocity between the radar and the ground is essentially zero. Clutter to either side of the perpendicular will have a relative-velocity component and hence some doppler frequency shift; consequently the clutter spectrum from the altitude return will be of finite width. The shape of the altitude return spectrum will depend upon the variation of the clutter cross section as a function of the grazing angle.

The clutter illuminated by the antenna sidelobes in directions other than directly beneath the aircraft may have any relative velocity from $+V_I$ to $-V_I$ depending on the angle made by the antenna beam and the aircraft velocity vector, as indicated by equation 6.12. The clutter spectrum contributed by these sidelobes will extend $2V_I/\lambda$ Hz on either side of the transmitter frequency. Although the shape of the spectrum has been shown in Figure 6.2b as uniform, it must be noted that the actual shape of this spectrum will depend both on the nature of the terrain illuminated and the shape of the antenna sidelobes.

The ground clutter directly illuminated by the main beam of the antenna is also shown in Figure 6.2b. This clutter "spike" is termed the main beam clutter spike. Its doppler shift is given by:

$$f_d = 2 \frac{V_I \cos \psi_I}{\lambda} \qquad (6.13)$$

It should be noted that the position of the main lobe clutter spike will change if the radar is scanning and also if the interceptor changes its velocity. Finally, Figure 6.2b illustrates the position of the target echo in the clutter frequency spectrum. The exact position of the target echo depends, of course, on its velocity relative to that of the interceptor. If the target is approaching the interceptor head-on then the doppler frequency shift of the target will be greater than

the doppler shifts on the clutter echoes. This is the situation that is illustrated in Figure 6.2b. As the relative position and relative velocity between the interceptor and target changes, the position of the target echo in the clutter frequency spectrum will change also.

This brings us to the problem of clutter interference. Clutter will interfere with recognition of the target during any of the following situations.

1. When the target doppler frequency coincides with the frequency of the mainlobe clutter spike.

2. When the target doppler frequency coincides with the altitude return clutter spike. This is termed "specular spike interference."

3. When the target doppler frequency enters the sidelobe clutter spectrum.

Whether or not clutter will interfere with the process of tracking a target depends on the actual mechanism used by the airborne radar to track the target and on the actual shape of the sidelobe clutter spectrum.

In order to determine the effects of the above three "clutter interference situations" on a given LAR diagram it is necessary to employ digital computer techniques to analyze the dynamic geometry of an air-to-air intercept. The above three "clutter interference situations" usually take the form of inequalities which must be satisfied during any given computer run.

Referring to the enlarged interceptor radar clutter spectrum in Figure 6.3, it can be seen that the interceptor tracks the target by centering a doppler filter bank about the target doppler frequency. As the target doppler moves toward the left, the filter bank moves with it; always keeping the signal somewhat centered. As the target doppler approaches the mainlobe clutter spike the target becomes indistinguishable "velocity wise" from the surrounding terrain. This is because the doppler filter cannot distinguish between the mainlobe clutter and the target return. How close the target doppler can actually approach the mainlobe clutter before the signal is obsecured, depends upon the size of the mainlobe spike and the necessary signal-to-noise ratio of the target return required for the tracking process in the interceptor. The point of minimum approach is usually expressed as a combination of the half bandwidths of the mainlobe clutter spike and the doppler filter bank.

Whether or not there will be interference between the mainlobe clutter spike and the target doppler may now be expressed as an inequality. There will be interference if the following inequality is satisfied in the AI radar.

$$-AIC + f_o - 2\frac{V_I \cos\psi_I}{\lambda} \leq f_o - 2\frac{R_{IT}}{\lambda} \leq AIC + f_o + 2\frac{V_I \cos\psi_I}{\lambda} \quad (6.14)$$

INTERCEPTOR HEAD ON CLUTTER SPECTRUM

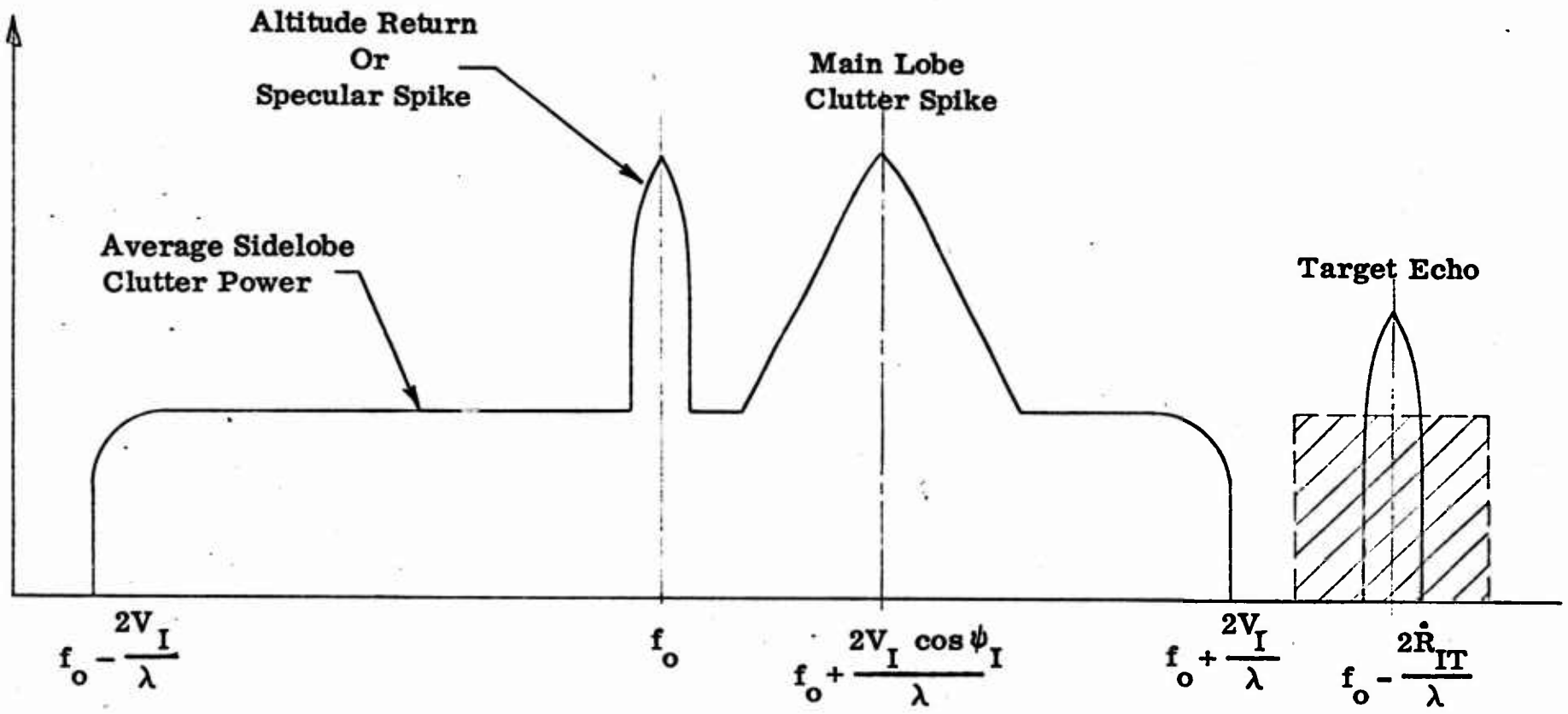

Figure 6.3

which can be reduced to:

$$-\frac{AIC}{2} \leq -\dot{R}_{IT} - V_I \cos\psi_I \leq \frac{AIC}{2} \qquad (6.15)$$

Where

AIC = Combination of the half-bandwidths of the mainlobe clutter spike and the doppler filter (ft/sec.)

ψ_I = Spatial angle between the interceptor target LOS and the interceptor velocity vector (as per Figure 6.2a)

$\dot{R}_{IT}$ = Interceptor-to-target closing rate (ft/sec.)

The other two clutter interference situations may also be expressed as inequalities. There will be interference between the target doppler and the altitude return if:

$$-\frac{A_{DMIN}}{2} \leq -\dot{R}_{IT} \leq \frac{A_{DMIN}}{2} \qquad (6.16)$$

Where

A_{DMIN} = Combination of the half-bandwidth of the specular spike and the doppler filter (ft/sec.)

$\dot{R}_{IT}$ = Interceptor-to-target closing rate.

Finally, there will be interference between the target doppler and the total clutter spectrum if:

$$E_I \leq 0 \text{ and } \dot{R}_{IT} > -V_I$$

$$E_I > 0 \text{ and } \dot{R}_{IT} > -V_I \cos E_I \qquad (6.17)$$

Where

E_I = Interceptor elevation angle.

It should be noted that the mainlobe clutter spike inequality does not exist

when the target is above the interceptor. In these situations the mainlobe of the radar does not impinge on the ground. Thus, there will be no mainlobe clutter.

It should also be mentioned that, for a given interceptor, all of the above three inequalities may not be applicable. For instance, one specific interceptor may not be able to track a target anywhere within the total clutter spectrum. In this case its clutter constraints would be expressed by equation 6.17. Another interceptor, though, may only loose track of the target after its doppler reaches the mainlobe clutter spike. In this case, its clutter constraints would be expressed by equation 6.15.

As a final consideration, it should be mentioned that clutter constraints (no matter what form they take) are only applicable during that part of an air-to-air intercept when the interceptor is required to illuminate a target. For missiles with a semiactive midcourse homing system and an active terminal homing system an interceptor is only required to illuminate the target during the midcourse phase of the missile's flight. It is during this time that the clutter inequalities are applicable.

6.2 SEMIACTIVE - MIDCOURSE PHASE GUIDANCE FACTORS

This section discusses three factors pertinent to the semiactive midcourse phase of a missle's flight, which influence its LAR diagram. These factors include:

1. Mainlobe and sidelobe seeker clutter
2. Semiactive seeker acquisition range
3. Effect of midcourse navigation law

6.2.1 Missile Seeker Clutter Spectrum

Recall the discussion of the doppler frequency observed by the AI radar as presented in Section 6.1. It was shown that the target doppler, as observed by the AI radar, was described by equation 6.9. This equation will not, however, describe the target doppler as observed by the semiactive missile radar seeker.

As illustrated by Figure 6.4, the line of sight between the missle and target, in general, does not coincide with the line of sight between the interceptor and target. This coupled with the fact that the missile speed is different than the interceptor speed acts to produce a different target induced doppler shift at the

veda

SEMI ACTIVE INTERCEPT GEOMETRY

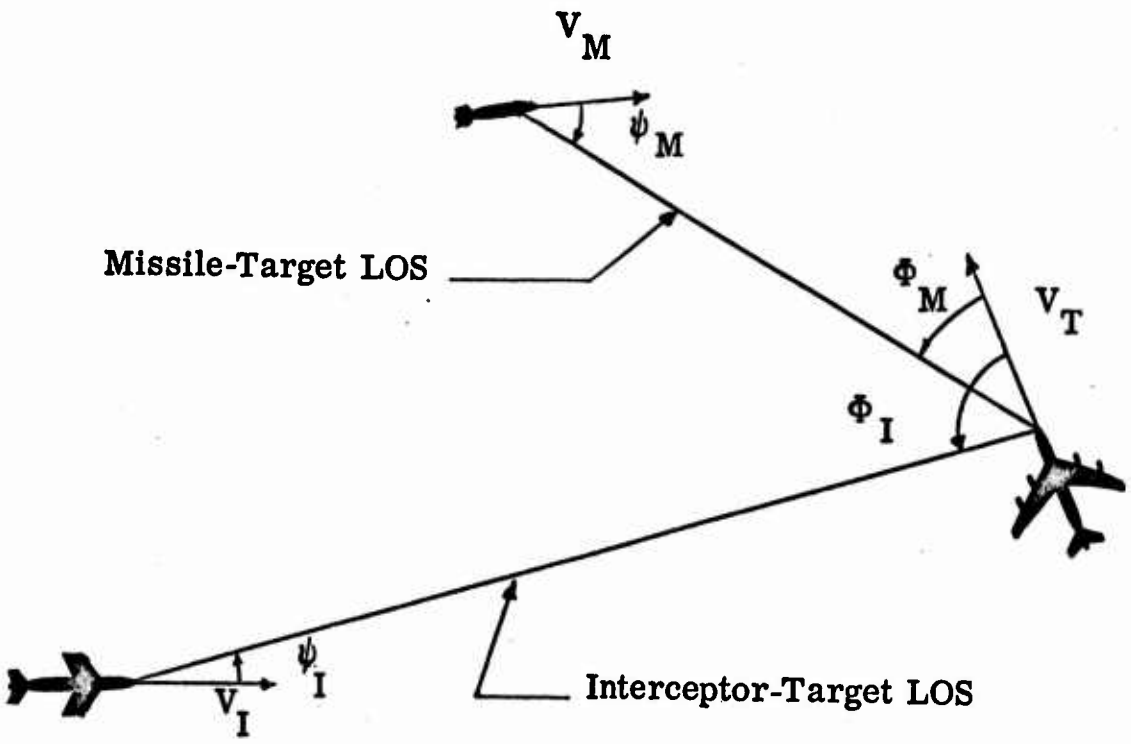

Figure 6.4

semiactive missile seeker. Recall equation 6.8 which described the shift in frequency that would be observed by a moving observer (target) from a moving transmitter (AI-radar). In terms of the nomenclature in Figure 6.4 equation 6.8 may be rewritten as:

$$f_d = \frac{V_I \cos \psi_I + V_T \cos \Phi_I}{\lambda} \qquad (6.18)$$

This equation describes the doppler frequency incident at the target, and is the same for both the AI radar and the missile seeker. The difference now arises because the reflected signal observed by the semiactive seeker arrives via the missile-target LOS. The relative velocity between the missile and the target acts to induce an additional doppler shift to the reflected signal. Employing the principles discussed in Section 6.1 and the reciprocity principle, the doppler shift observed by the semiactive missile seeker is found to be:

$$f_{dM} = \frac{-V_I \cos \psi_I - V_T \cos \Phi_I - V_I \cos \Phi_M - V_M \cos \psi_M}{\lambda} \qquad (6.19)$$

This may be rewritten in terms of interceptor-to-target and missile-to-target closing rates as:

$$f_{dM} = - \frac{\dot{R}_{IT}}{\lambda} - \frac{\dot{R}_{MT}}{\lambda} \qquad (6.20)$$

Now that the doppler shift observed by the semiactive seeker has been developed it is possible to examine the clutter spectra observed by the seeker. The semiactive seeker clutter bandwidth may be determined in the same manner as it was for the AI radar. Namely, by considering all values of ψ_I and ψ_M (interceptor and missile heading) between $+\pi$ and $-\pi$. Again, this is all the terrain between the read and forward horizons for horizontal velocities V_M and V_I. The clutter bandwidth, illustrated in Figure 6.5, are those frequencies, f, which satisfy

$$f_o - \frac{V_I + V_M}{\lambda} \leq f \leq f_0 + \frac{V_I + V_M}{\lambda} \qquad (6.21)$$

It is evident by comparing equation 6.12 (the AI radar clutter bandwidth) with equation 6.21, that the bandwidth of the clutter in the missile seeker is wider than that in the AI radar. It is wider by an amount equivalent to the increase in missile speed over the interceptor speed. Besides this difference the clutter spectra differ in two other respects. Comparing Figure 6.5 with Figure 6.3, we note that only one mainbeam clutter band occurs in the AI radar while two such bands occur in the seeker spectrum. Secondly, the main beam clutter in the radar depends only on the interceptor speed while both mainbeam bands in the

MISSILE SEEKER SEMI-ACTIVE PHASE CLUTTER SPECTRUM

$$\text{I: } f_o + \frac{V_I \cos E}{\lambda} + \frac{V_M \cos F}{\lambda}$$

$$\text{II: } f_o + \frac{V_I \cos C}{\lambda} + \frac{V_M \cos \psi_M}{\lambda}$$

$$\text{III: } f_o + \frac{V_I \cos \psi_I}{\lambda} + \frac{V_M \cos A}{\lambda}$$

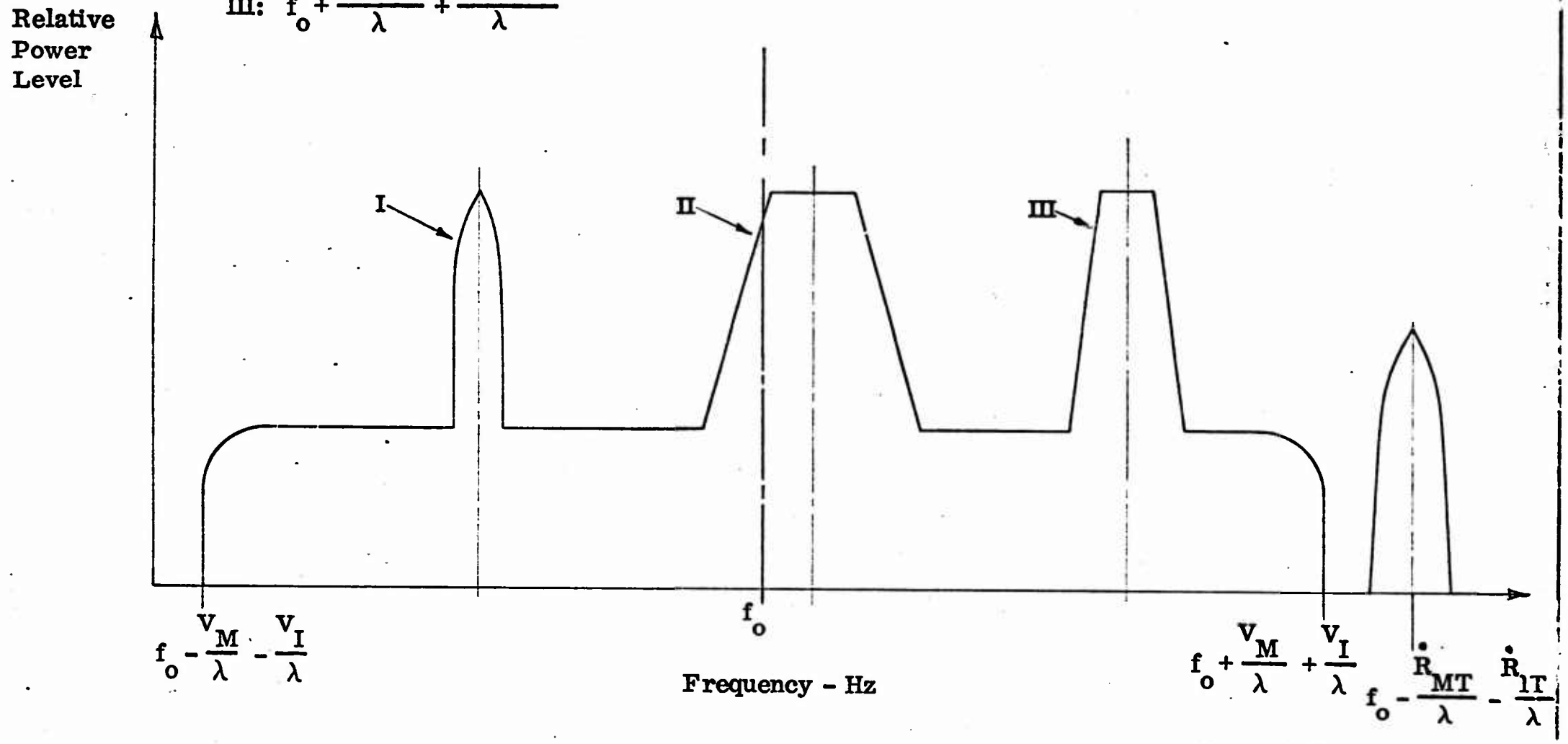

Figure 6.5

veda INCORPORATED

seeker depend on missile speed as well as interceptor speed. This means that avoiding main beam clutter in the radar does not necessarily mean that mainbeam clutter is also avoided in the seeker. The clutter free target dopplers in both the AI radar and missile seeker depend on the relative geometries of the interceptor, missile and target throughout the intercept. Therefore, the clutter analysis must again be investigated through the use of inequalities which must be satisfied by the missile during the semiactive phase of its flight.

Before describing these inequalities or "clutter tests" it is necessary to develop geometrical relationships which describe the various reflective paths that produce both the main beam clutter spikes and the specular spike in the semiactive missile seeker. From Figure 6.6 these paths are:

1. From an AI radar sidelobe to a point on earth in line with the missile target LOS (path 1 on Figure 6.6, and return via the missile-target LOS through the missile seeker main beam (path 2 on Figure 6.6.)

2. From the AI Radar mainlobe to a point on earth in line with the interceptor-target LOS (path 3 on Figure 6.6), and return via a missile seeker sidelobe (path 4on Figure 4.)

3. From an AI radar sidelobe to a point on earth (path 5 on Figure 6.6) and return via a missile seeker sidelobe (path 6 on Figure 6.6), where both the angle of incidence and reflection are the same. This is the semiactive phase specular return path.

In order to determine the frequencies at which each of the above spikes occur, certain angles are necessary. These angles are defined as follows:

ANGLE	DEFINITION
A	The spatial angle between the missile velocity vector and the seeker sidelobe path which results from interceptor mainlobe illumination (path 4 on Figure 6.6).
ψ_I	The spatial angle between the interceptor velocity vector and the interceptor target LOS
C	The spatial angle between the interceptor velocity vector and the AI radar sidelobe clutter path (path 1 on Figure 6.6).
ψ_M	The spatial angle between the missile velocity vector and the missile target LOS.
E	The spatial angle between the interceptor velocity vector and the AI radar sidelobe path that results in semiactive specular reflection in the missile (path 5 on Figure 6.6).

veda
INCORPORATED

MISSILE SEMI-ACTIVE SEEKER CLUTTER GEOMETRY

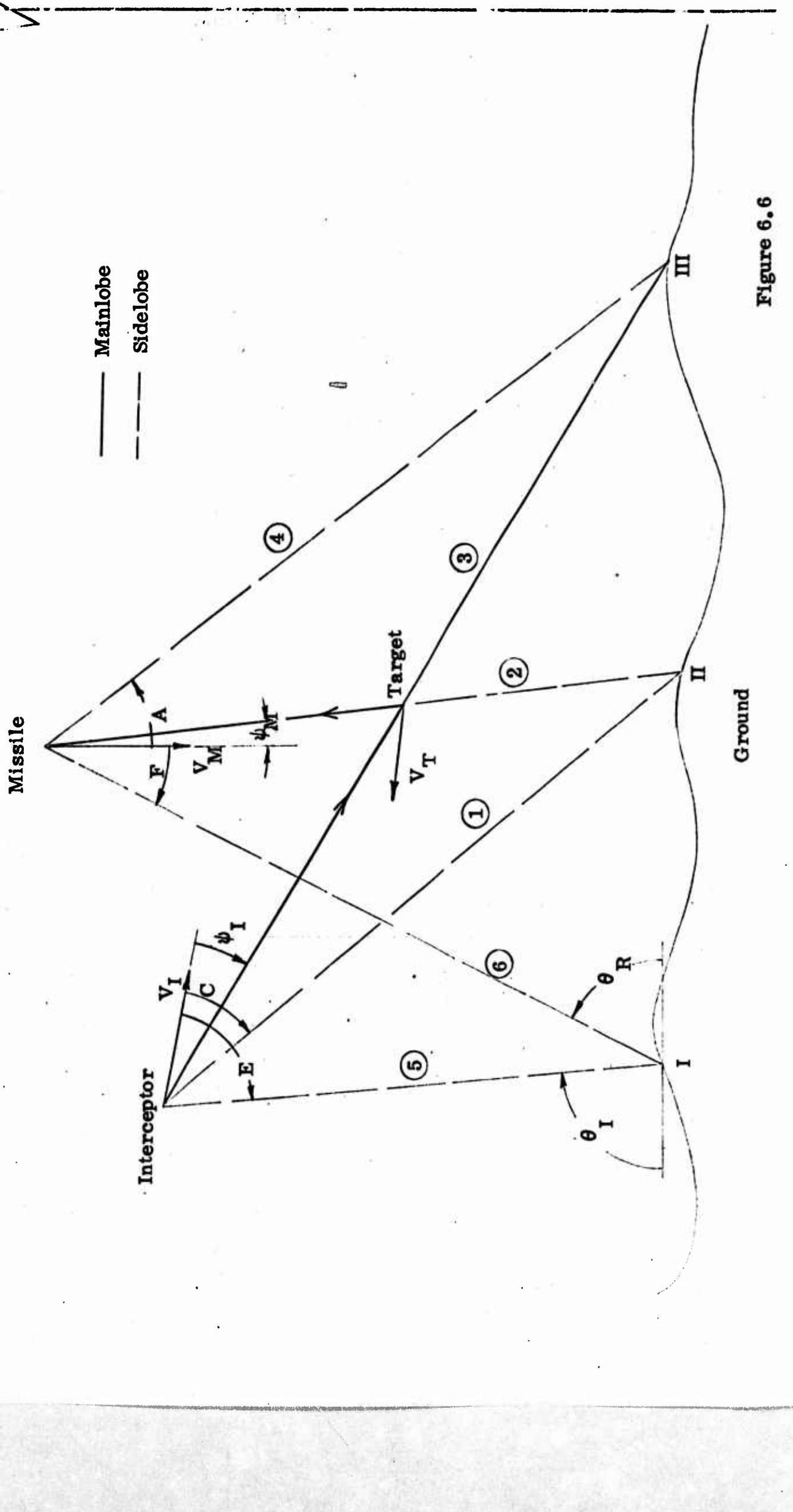

Figure 6.6

veda INCORPORATED वेद

ANGLE	DEFINITION
F	The spatial angle between the missile velocity vector and the seeker sidelobe path which results in semiactive specular reflection in the missile (path 6 on Figure 6.6).

The interested reader is referred to reference 4 where these angles are derived as a function of the attack geometry.

The frequencies at which the spikes occur in the semiactive seeker clutter spectra may be determined in the same manner that the frequency of the mainlobe clutter spike was determined for the AI radar. The frequencies at which the clutter spikes occur are given as follows:

1. Specular Spike

$$f_c = f_o + \frac{V_I \cos E + V_M \cos F}{\lambda} \qquad (6.22)$$

2. Interceptor Mainlobe - Missile Sidelobe

$$f_c = f_o + \frac{V_I \cos \psi_I + V_M \cos A}{\lambda} \qquad (6.23)$$

3. Interceptor Sidelobe - Missile Mainlobe

$$f_c = f_o + \frac{V_I \cos C + V_M \cos \psi_M}{\lambda} \qquad (6.24)$$

The position of these spikes in the semiactive seeker clutter spectrum is qualitatively illustrated in Figure 6.5. The position of the target doppler is also illustrated for the case where the missile is approaching the target head-on. As for the AI radar, the relative positions of the target doppler, the specular spike and the two mainlobe clutter spikes will vary with changes in the relative position and relative velocity between the interceptor, target and missile throughout an intercept.

From the discussion in Section 6.1, it will be remembered that as the target doppler approaches the specular spike, or either of the two mainlobe clutter spikes, or even possibly the total clutter spectrum, the target may become indistinguishable

"velocity wise" from the surrounding terrain. Just how close the target doppler can approach these spikes before the missile looses track on the target depends on the width of the missile's velocity tracking filters as well as the size of the spikes and various mechanics of the tracking process within the missile. To determine whether or not clutter interferes with the target tracking process and therefore effects the missile's LAR it is necessary to simulate the intercept and employ "clutter tests". These clutter tests are listed below. However, before listing them, the derivation of a typical test will be illustrated.

There may be interference between the target doppler signal and the interceptor mainlobe-missile sidelobe clutter path if the following inequality is satisfied during the semiactive phase of a missile flight.

$$f_o + \frac{V_I \cos \psi_I}{\lambda} + \frac{V_M \cos A}{\lambda} - \frac{MC}{\lambda} \leq f_o - \frac{\dot{R}_{MT}}{\lambda} - \frac{\dot{R}_{IT}}{\lambda} \leq$$

$$f_o + \frac{V_I \cos \psi_I}{\lambda} + \frac{V_M \cos A}{\lambda} + \frac{MC}{\lambda} \qquad (6.25)$$

or if

$$-MC < -\dot{R}_{MT} - \dot{R}_{IT} - V_I \cos \psi_I - V_M \cos A \leq MC \qquad (6.26)$$

where $\dot{R}_{MT}$, $\dot{R}_{IT}$, V_I, V_M, A and ψ_I have been defined previously and where MC represents a combination of the half bandwidths of the clutter spike and the doppler filter (MC is expressed in ft/sec.)

The other three tests are:

1. Specular spike

$$-S_{DMIN} \leq -\dot{R}_{MT} - \dot{R}_{IT} - V_I \cos E - V_M \cos F \leq S_{DMIN} \qquad (6.27)$$

Where

S_{DMIN} = Combination of the half bandwidths of the specular spike and the doppler filter (ft/sec.)

2. Interceptor Sidelobe - Missile Mainlobe clutter spike

$$-MC \leq -\dot{R}_{MT} - \dot{R}_{IT} - V_T \cos C - V_M \cos \psi_M \leq MC \qquad (6.28)$$

Where

MC = Combination of the half bandwidths of the clutter spike and doppler filter (ft/sec).

3. Clutter Spectrum Limits

If

$E_M \leq 0$, $E_I \leq 0$, and $\dot{R}_{MT} + \dot{R}_{IT} > -V_M - V_I$

$E_M \leq 0$, $E_I > 0$, and $\dot{R}_{MT} + \dot{R}_{IT} > -V_M - V_I \cos E_I$

$E_M > 0$, $E_I \leq 0$, and $\dot{R}_{MT} + \dot{R}_{IT} > -V_M \cos E_M - V_I$

$E_M > 0$, $E_I > 0$, and $\dot{R}_{MT} + \dot{R}_{IT} > -V_M \cos E_M - V_I \cos E_I$

Where

E_M and E_I are the elevation angles of the missile and interceptor respectively.

Even though the clutter problem depends on the relative positions and velocities of the missile, interceptor and target during an intercept and cannot be analyzed in depth without the aid of computing devices, doppler exclusion regions may be drawn on a LAR diagram provided certain assumptions are made. Dopper exclusion regions are defined as those regions on a LAR diagram within which the missile may not be able to track the target because of mainlobe and sidelobe clutter.

Before illustrating the procedure by which doppler exclusion regions are drawn on a LAR diagram, it is necessary to single out some of the assumptions involved. First it will be assumed that the missile tracks the target by keeping its doppler centered in a doppler filter bank of bandwidth B Hz. In other words, the filter is centered $\pm B/2$ about the target doppler.

There are two situations in which the doppler filter cannot distinguish between the target return and interfering signals (clutter) and both of these are pertinent to clutter analysis. First, if only part of the filter bank is subjected to extreme interference (mainlobe clutter) the doppler filters cannot distinguish between the target return and the interference. The second situation is when the interference increases sharply from an average value in some part of the filter. This could be caused by "spikey" side lobe clutter. In this situation also, the doppler filters cannot distinguish between the interfering signals and the target return.

The first situation is of primary interest in drawing doppler exclusion regions. The mainlobe clutter interference acts to exclude all the region in a LAR within which the target return lies less than half the bandwidth of the doppler filter bank away from the edge of the mainlobe clutter. In other words, only those geometries such that the target return lies at least $B/_2$, away from the edge of the mainlobe clutter can be used as permissible attack conditions. This exclusion bandwidth is equated to a minimum target induced doppler along the line of sight by:

$$f_d = 2 \frac{\Delta V_D}{\lambda} \tag{6.30}$$

but $f_d = B/_2$, therefore,

$$\Delta V_D = \frac{B/_2 \times \lambda}{2} \tag{6.31}$$

Where

ΔV_D = minimum target induced doppler along LOS (ft./sec.)

B = bandwidth of doppler filter bank (Hz).

λ = wavelength of transmitted signal (feet).

For instance, if the bandwidth of the doppler filter bank was 20 kHz and the radar transmission frequency was X-band ($\lambda = 0.1$ feet), then the doppler exclusion bandwidth would be equivalent to 500 ft/sec. of target induced velocity along the LOS.

The final doppler exclusion bandwidth of approximately 500 ft/sec (for this particular case) may be shown on a LAR diagram by the following procedure. Since the target induced doppler along the LOS is given by:

$$\Delta V_D = V_T \cos \delta \tag{6.32}$$

Then the angle δ which defines the doppler exclusion region is given by:

$$\delta = \cos^{-1} \left(\frac{\Delta V_D}{V_T} \right) \qquad (6.33)$$

The angle δ defines a fan shaped region around the target which the missile must not penetrate. This fan shaped region or doppler exclusion region may be drwan on an aerodynamic launch range boundary as shown in Figure 6.7. If no other missile system constraints come into play, then the LAR diagram has been specified.

One constraint that may affect the above mentioned LAR diagram, is the seeker acquisition range of a semiactive missile. This factor is discussed in the following section.

6.2.2 Semiactive Seeker Acquisition Range

The range at which the semiactive missile seeker can be expected to acquire a target depends upon the strength of the reflected RF signal at the missile seeker. Since the strength of this signal is a probabilistic function of many factors, the semiactive seeker acquisition range is usually defined as that range to the target where the probability of successfully acquiring the target is very high (given certain specified constraints.)

The semiactive seeker acquisition range is one of the factors which influence the maximum launch range boundry on a LAR diagram. Since the missile seeker must be able to acquire the target shortly after launch, the missile must be launched within a circle of radius R_s (seeker acquisition range) centered at the position of the target at launch. This is illustrated in Figure 6.8 where the seeker acquisition range fixes the maximum launch range of the missile in the forward hemisphere of the LAR (since it is less than the maximum aerodynamic range of the missile.)

MISSILE SEEKER ACQUISITION RANGE

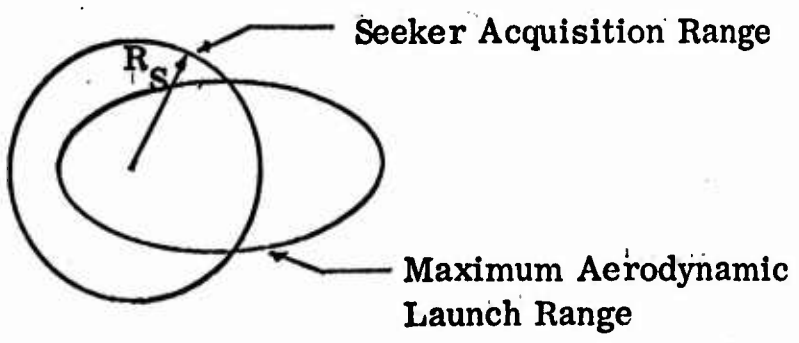

FIGURE 6.8

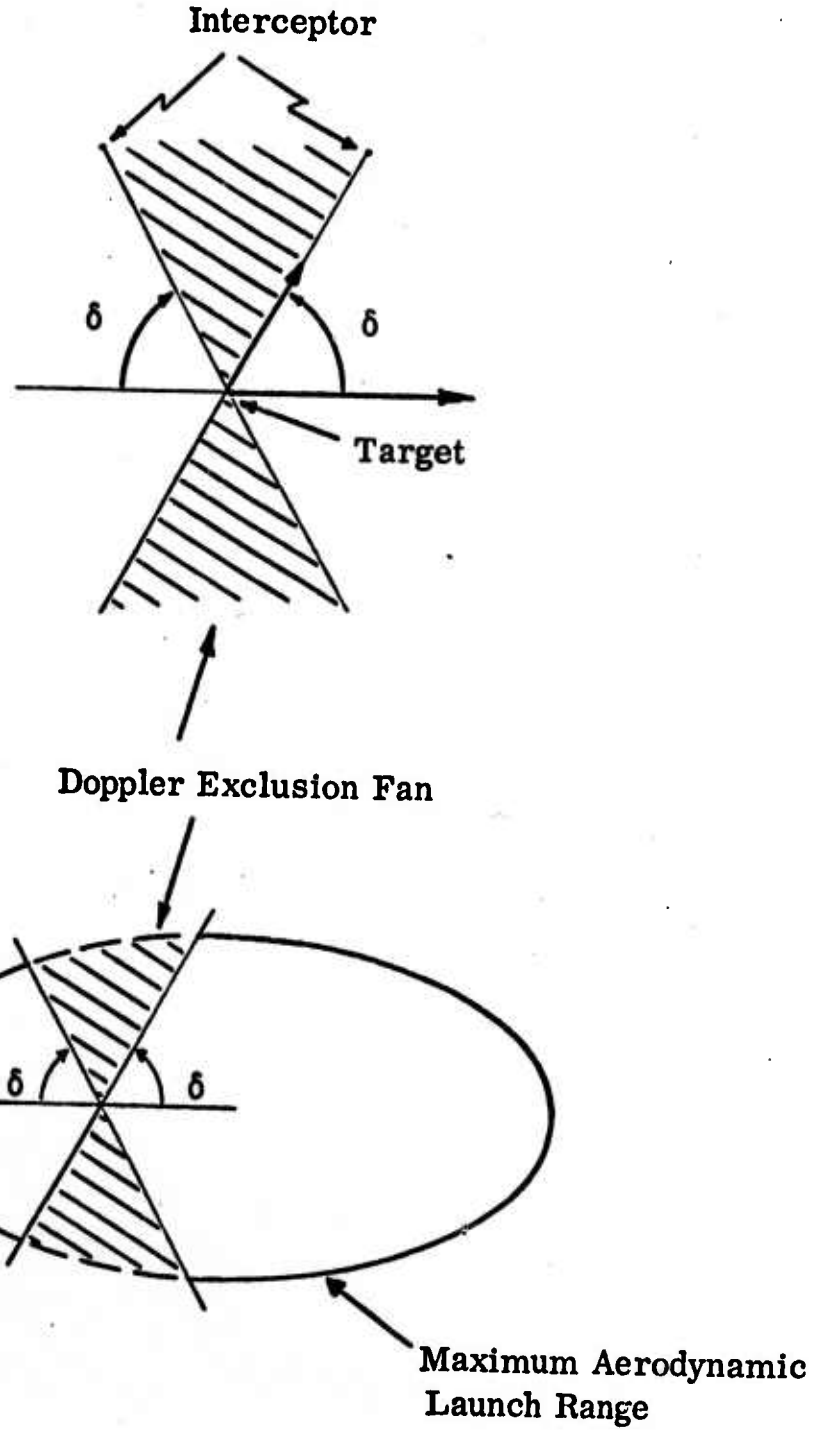

DOPPLER EXCLUSION REGION

Figure 6.7

6.2.3 Effect Of Missile Navigation Law

Section 5.2 discussed the effect of missile seeker gimbal limits on LAR diagrams for long-range boost-glide air-to-air missiles. That discussion dealt specifically with missiles that employ proportional navigation for their midcourse navigation law. It will be remembered that since proportional navigation attempts to keep the missile-target LOS from rotating, the missile turns toward the LOS during its thrusting phase and turns away from the LOS during its glide phase. This phenomenon may force the missile into a terminal hooking maneuver which results in missile-to-target gimbal angles that are beyond the capability of the missile seeker. To alleviate this, the missile launch range had to be decreased so as to increase the average missile velocity during an intercept. This phenomon was reflected in the missile's LAR diagram (against low altitude targets) by a maximum launch range that rapidly decreased with increasing aspect angle.

In order to illustrate the effect the midcourse navigation law can have on a LAR diagram, consider the same long-range, boost glide missile - but change the midcourse navigation law to deviated pursuit. Deviated pursuit, it will be recalled, attempts to maintain a constant lead angle between the missile X- axis and the missile-to-target LOS. The LOS does not remain fixed in space as it does with proportional navigation, but rather it rotates in a manner that causes the target aspect angle to reduce with time. In other words, the missile now flies to a position in front of the target. Deviated pursuit therefore, by controlling only the lead angle makes the missile's trajectory insensitive to variations in missle velocity. Since the trajectory is no longer sensitive to variations in velocity, the missile is not required to turn in order to counteract changes in missile velocity. This fact is illustrated by the typical maneuver acceleration profiles for deviated pursuit and proportional naigation in Figure 6.9. It is important to note from the acceleration profiles that since the average maneuver acceleration is less for deviated pursuit than for proportional navigation, the degradation in missile velocity due to induced drag will also be less. This follows because induced drag is directly related to the missile's normal acceleration, and induced drag acts to decrease missile velocity.

All the above characteristics are reflected in a LAR diagram for deviated pursuit (illustrated in Figure 6.10). The most important fact to note from the LAR is that maximum missile launch range remains relatively constant with aspect angle for deviated pursuit, (providing, of course, that the seeker acquisition range establishes the maximum launch range boundary on the LAR). This is to be compared to the same attack conditions using proportional navigation, where maximum launch range decreased with aspect angle.

ACCELERATION PROFILE COMPARISON

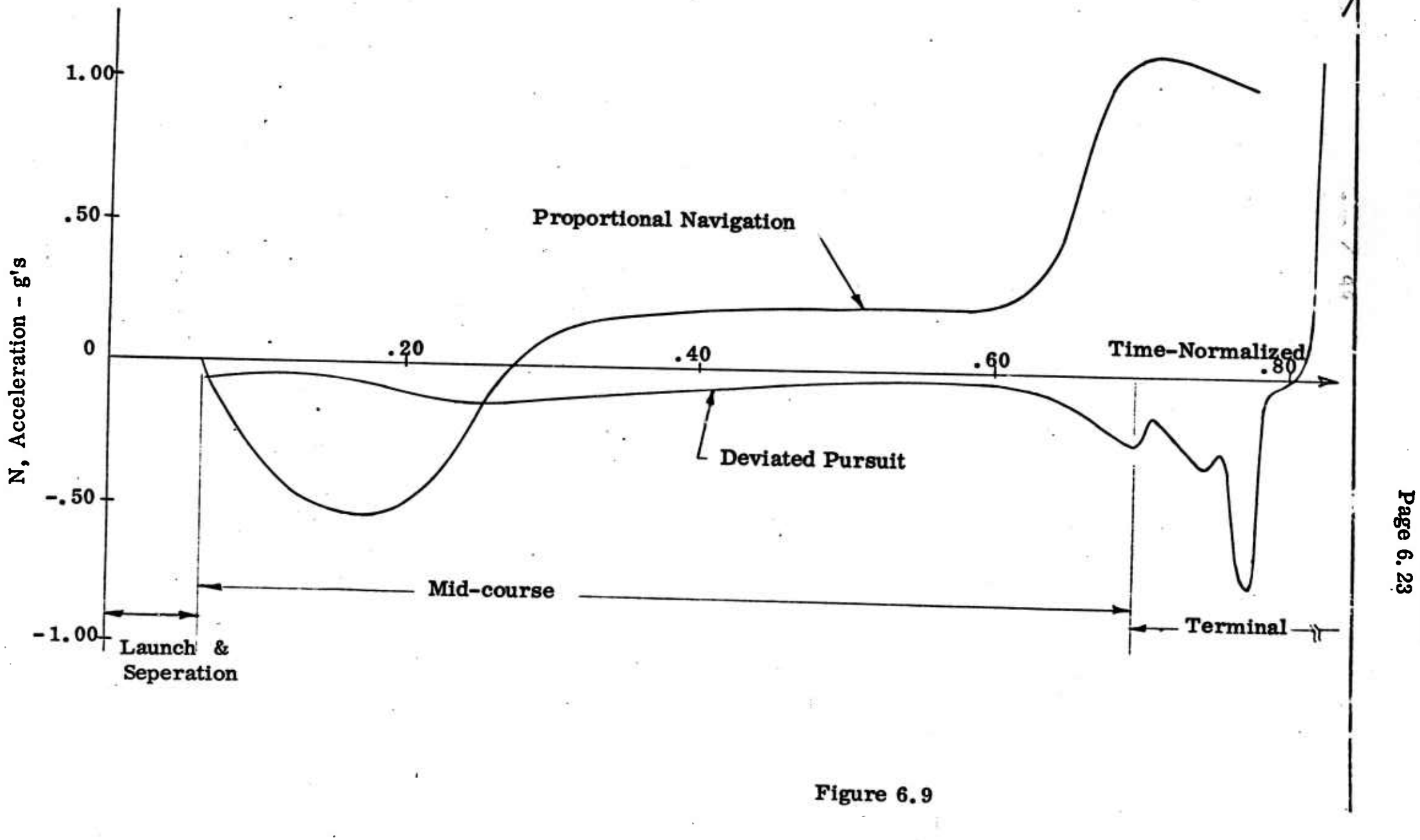

Figure 6.9

LAR COMPARISON

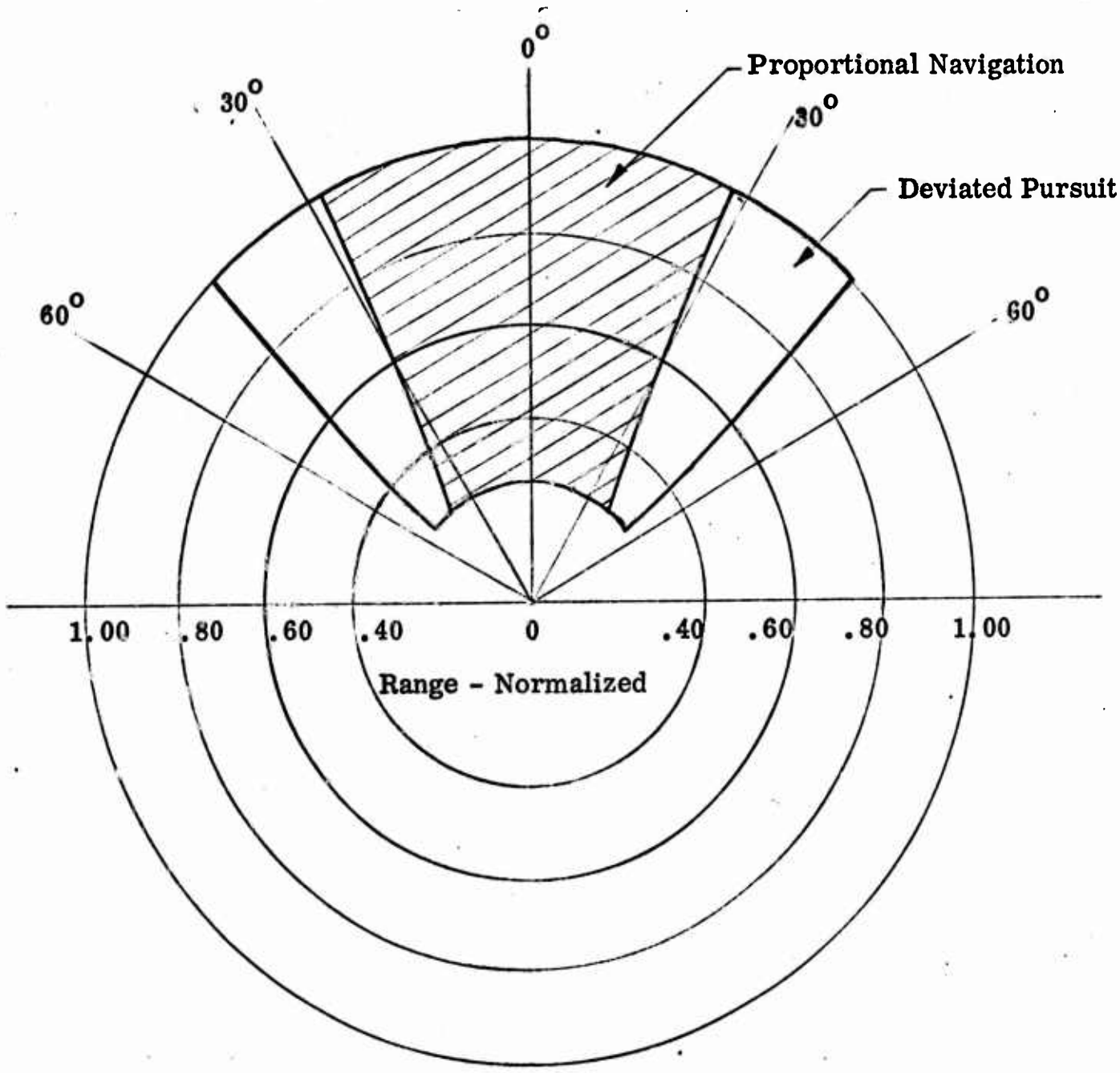

Target: Sea Level

Interceptor: 35,000 Ft.

Figure 6.10

6.3 ACTIVE-TERMINAL PHASE GUIDANCE FACTORS

This section discusses two factors pertinent to the active terminal phase of the intercept which influence a missile's LAR diagram. These factors include:

1. Mainlobe and sidelobe seeker clutter
2. Eclipsing effects
   a. seeker blind range
   b. minimum closing rate.

6.3.1 Mainlobe and Sidelobe Active Seeker Clutter

In many respects the missile seeker active phase clutter spectrum is similar to the AI radar clutter spectrum. Since the interceptor is not required to illuminate the target there is only one mainlobe spike in the active missile clutter spectrum as opposed to two in the semiactive phase clutter spectrum. As was the case for the interceptor, this mainlobe clutter spike is the result of the mainbeam of the seeker antenna impinging on the earth. The doppler shift of the mainbeam clutter spike depends, in this instance, on the velocity of the missile and is given by:

$$f_d = 2 \frac{V_M \cos \psi_M}{\lambda} \tag{6.34}$$

The clutter bandwidth (or spectrum of received signals) for an active pulse modulated missile seeker are those frequencies, f, which satisfy:

$$f_o - 2\frac{V_M}{\lambda} \leq f \leq f_o + 2\frac{V_M}{\lambda} \tag{6.35}$$

The clutter spectrum again was determined by considering all the terrain (illuminated by the seeker sidelobes) between its rear and forward horizons (i.e. all values of ψ_M between $+\pi$ and $-\pi$). The geometry and the clutter spectrum are illustrated in Figures 6.11a and 6.11b, respectively. It will be noted from Figure 6.11b, that the active phase seeker clutter spectrum is wider than either the AI radar clutter spectrum or the semiactive phase seeker clutter spectrum. This, of course, results from the fact that the velocity of the missile is higher than that of the interceptor.

vəda INCORPORATED

MISSILE SEEKER ACTIVE CLUTTER GEOMETRY

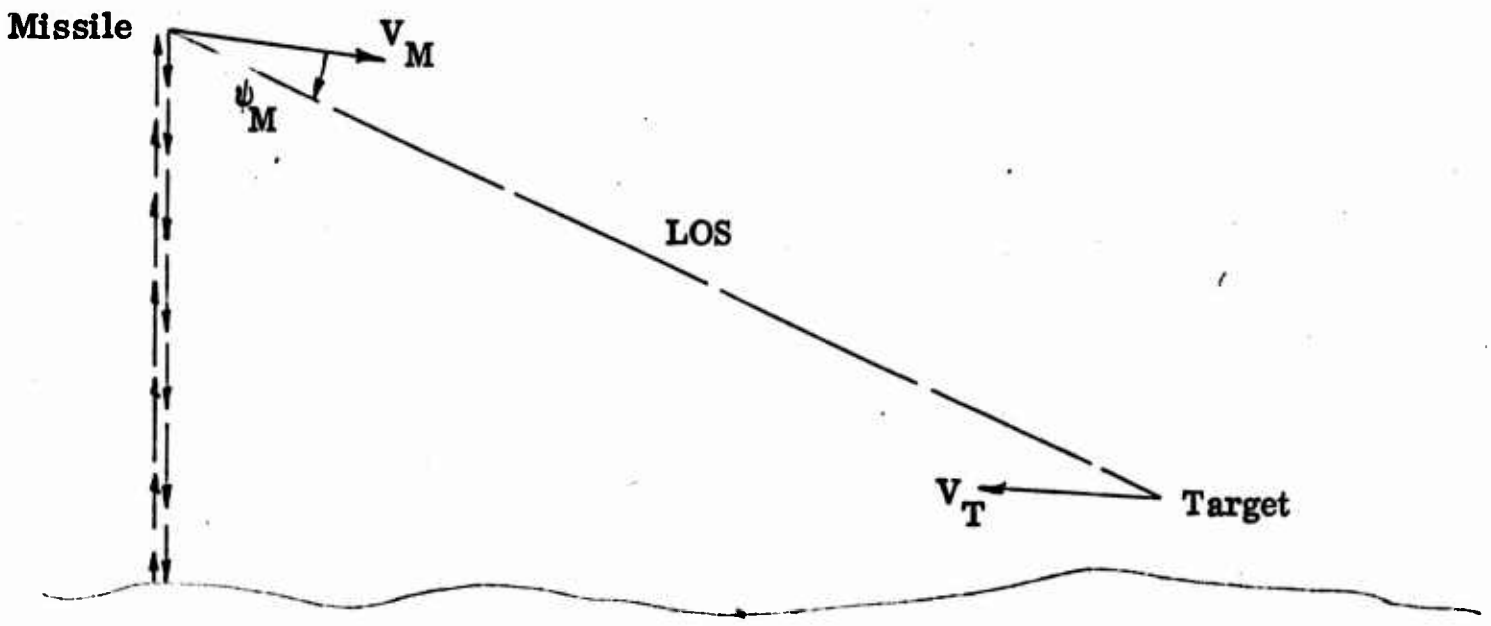

Figure 6.11 a

MISSILE SEEKER ACTIVE CLUTTER SPECTRUM

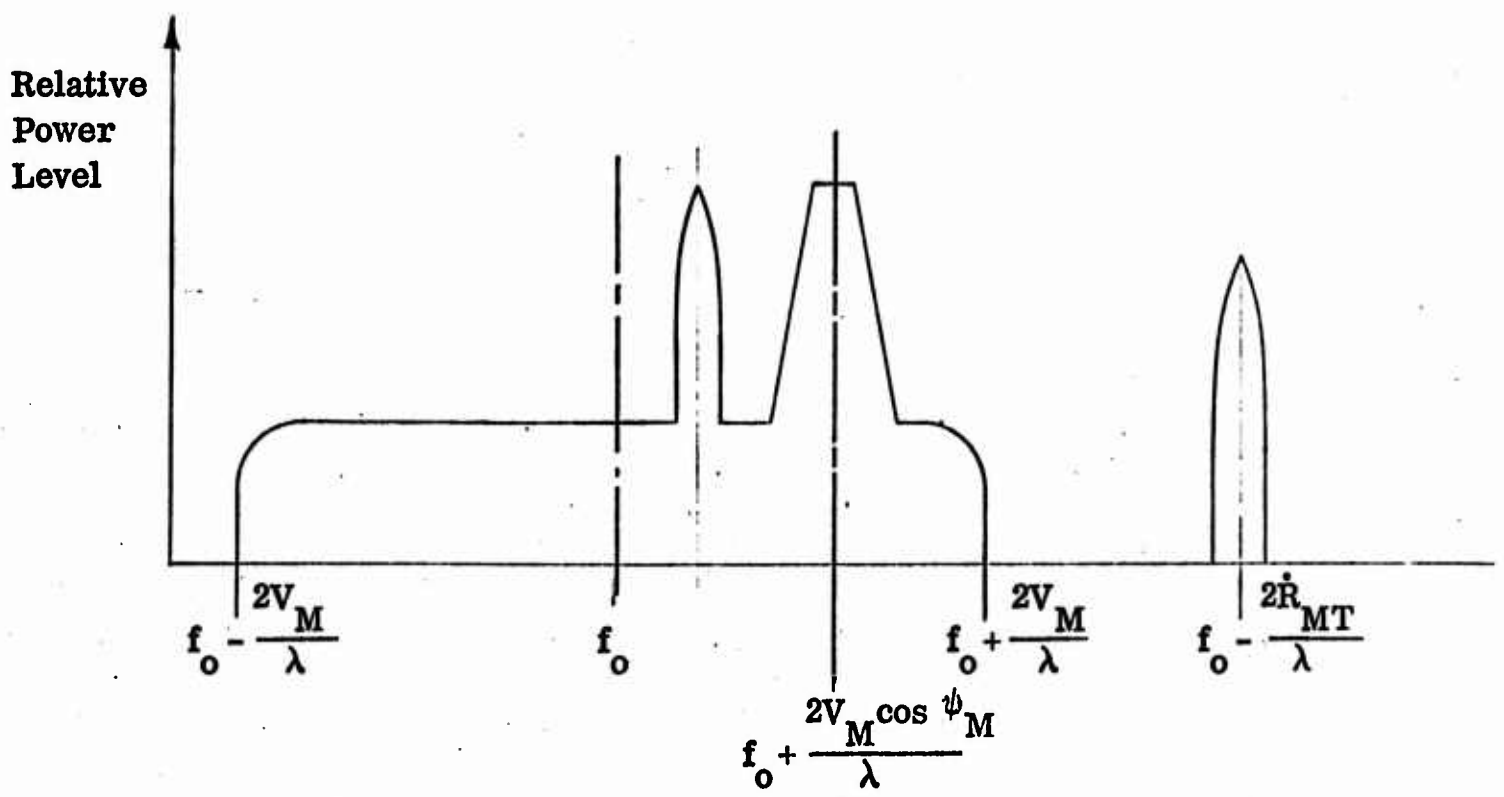

Figure 6.11 b

The position of the target doppler in the frequency spectrum is also shown in Figure 6.11b for a head-on intercept. The target doppler in this case is given by:

$$f_d = -2 \frac{\dot{R}_{MT}}{\lambda} \tag{6.36}$$

Now as for the previous cases, as the relative geometry and velocity between the missile and target changes, the position of the target doppler will change. Again, the possibility of clutter interference exists during an intercept so that it is necessary to derive clutter inequalities to test for this interference. These tests are listed as follows:

1. There will be interference between the target doppler and the active phase specular clutter spike if the following relationship is satisfied during the active phase:

$$\dot{R}_{MT} > - \frac{S_{DMIN}}{2} \tag{6.37}$$

where

S_{DMIN} = a combination of the half bandwidths of the specular spike and the doppler filter (ft/sec.)

2. There will be interference between the target doppler and the mainbeam clutter spike if the following relationship is satisfied during the active phase:

$$-\frac{MC}{2} \leq -\dot{R}_{MT} - V_M \cos \psi_M \leq \frac{MC}{2} \tag{6.38}$$

where

MC = A combination of the half bandwidths of the mainbeam spike and the doppler filter (ft/sec.)

3. There will be interference between the target doppler and the total clutter spectrum if:

$$\begin{aligned} E_M &\leq 0 \text{ and } \dot{R}_{MT} > - V_M \\ E_M &> 0 \text{ and } \dot{R}_{MT} > - V_M \cos E_M \end{aligned} \tag{6.39}$$

where

E_M = Missile Elevation angle

The clutter tests, presented above, were derived in the same manner as the clutter tests for the AI radar clutter spectrum and the missile seeker semiactive seeker clutter spectrum.

6.3.2 Terminal Phase Eclipsing Effects

If the missile employs an active pulse modulated type radar system during the terminal phase of the encounter, it will reach a range (near impact) beyond which it will no longer be able to track the target. This range is termed "radar blind range" and the phenemon itself is termed "eclipsing."

Eclipsing becomes a problem with a pulse modulated radar when a single antenna is used for both transmitting and receiving. When the antenna is used for transmitting the receiver is turned off so as to avoid the possibility of damage. Consequently, if the receiver is turned off when a reflected signal arrives at the antenna, no information can be obtained. This effect will occur whenever the missile-to-target range is such that the period between transmission and reception is an integral multiple of the pulse repitition period (i.e. the receiver is turned off or eclipsed at these ranges). The missile will therefore pass through regions during the encounter where it will not be able to see the target. This is not a severe problem, though, because the missile passes through these regions rapidly and because guidance commands may be extrapolated through them.

However, problems do arrise when the missile reaches the blind region centered around the target (blind range). This blind range may be estimated to vary between:

$$0.25\ \tau_p C \leq R_B \leq 1.0\ \tau_p C \qquad (6.40)$$

where

τ_p = width of transmitted pulse

C = velocity of light

The missile will, therefore, not be able to obtain information from the target during the final intercept phase of the encounter. This could result in large miss distances. The magnitude of the miss distance is related to the length of time the missile is blind, which, in turn, is related to the final missile to target closing rate by:

veda INCORPORATED

$$t_B = \frac{R_B}{\dot{R}_{MT}} \qquad (6.41)$$

where

t_B = Time missile is without guidance information due to eclipsing.

R_B = Missile seeker blind range

$\dot{R}_{MT}$ = Terminal missile-to-target closing rate.

The time the missile is blind should be less than a missile time constant (τ_r as discussed in Section 4.1.4). Since the missile will take this long to respond to its last command. If the time the missile is blind is longer than a missile time constant, then the missile will respond to its last command and continue on in that direction. Due to guidance noise and target maneuvers the miss distance performance will degrade rapidly beyond this point. As mentioned in Section 4.1.4, missile response times vary between 0.25 and 2.0 seconds for contemporary missile systems.

This phenemon may be reflected in the missile's LAR by placing a limit on the acceptable missile-to-target closing rate during the terminal phase. The minimum acceptable closing rate is:

$$\dot{R}_{MT\,(MIN)} \geq \frac{R_B}{\tau_r} \qquad (6.42)$$

If the missile-to-target closing rate falls below this minimum value during the terminal phase of the encounter, then the trajectory results in unacceptable performance. The launch range must, then, be reduced until acceptable performance is obtained.

This phenomenon acts to decrease the maximum launch range of the missile at higher aspect angles for low altitude targets where terminal closing rates are characteristically low. The maximum launch range of the missile in the rear hemisphere of the LAR is also degraded by terminal phase eclipsing effects.

veda INCORPORATED वेद

SECTION 7.0

SUMMARY

As mentioned in the Introduction, an air-to-air missile has three basic requirements. Namely, the missile homing guidance system must be able to track the target. The missile must be capable of traveling from the launch point to the impact point. Finally, it must arrive at the intercept point with sufficient maneuverability to reduce the final miss distance to within the lethal radius of its warhead.

As has been illustrated in the previous sections of this report, the various features of an air-to-air missile that implement these requirements, affect its performance (as measured by a LAR diagram). The various factors and constraints that influence a missile's LAR diagram may now be summarized.

I. Geometric Constraints

- A. AI Radar Gimbal Limits (for semiactive homing missile)
- B. Seeker Gimbal Limits
- C. Missile Climb and Dive Angle Limits

II. Guidance Constraints

- A. AI Radar Clutter Spectra Limits
- B. Semiactive Seeker Clutter Spectra Limits
- C. Active Seeker Clutter Spectra Limits
- D. Terminal Phase Missile-to-Target Range Rate Limits
- E. Semiactive Seeker Acquisition Limit
- F. Missile Guidance Laws and Trajectory Shape.

veda INCORPORATED वेद

III. Aerodynamic Constraints

A. Maximum Aerodynamic Launch Range

B. Minimum Missile Maneuver Limits

C. Maximum Missile Maneuver Limits

The effects of these constraints on a typical LAR diagram are illustrated in Figure 7.1.

veda INCORPORATED

LAR FORMATION

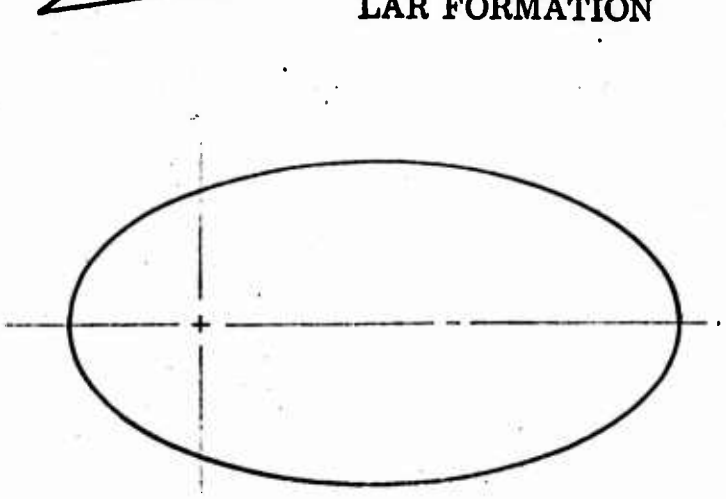

1) Aerodynamic Launch Range

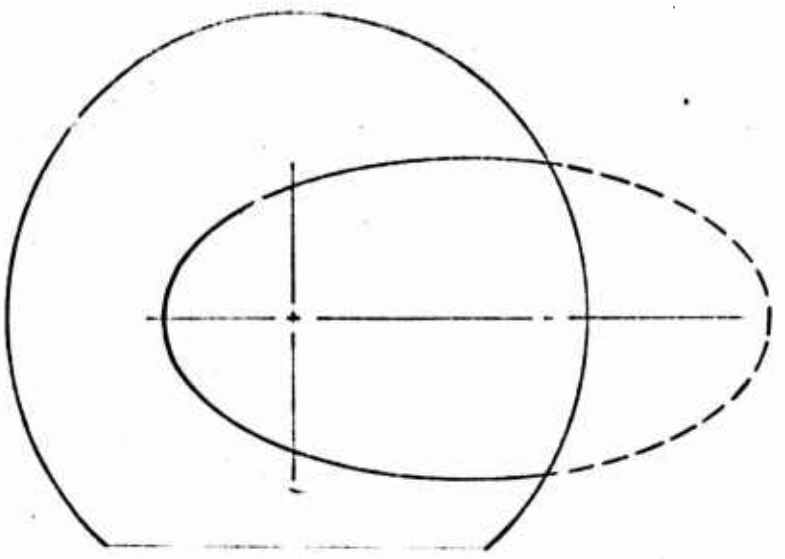

2) Seeker Limit

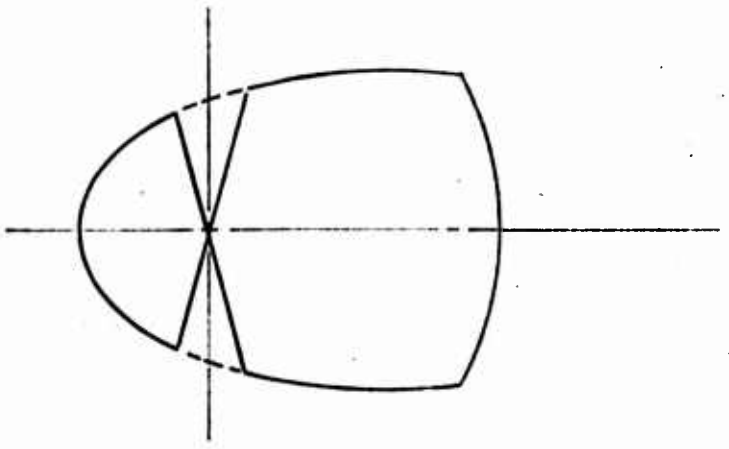

3) Doppler Exclusion Limit

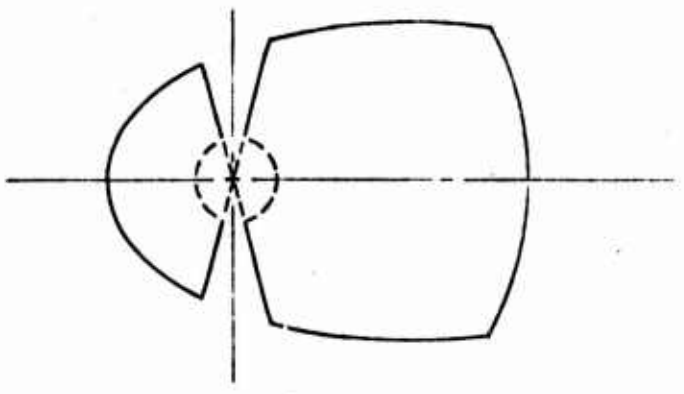

4) Minimum Range Limit

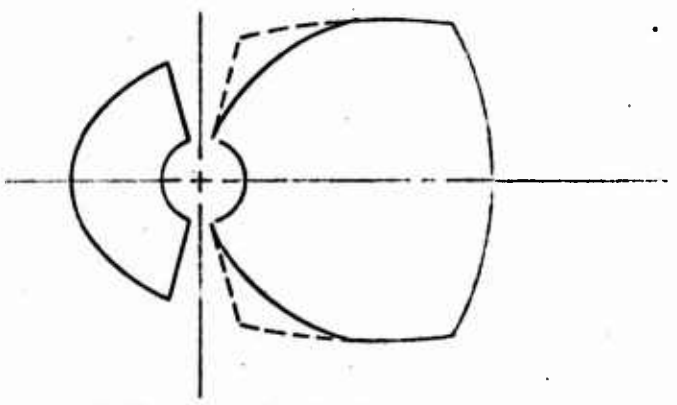

5) Seeker Gimbal Limit

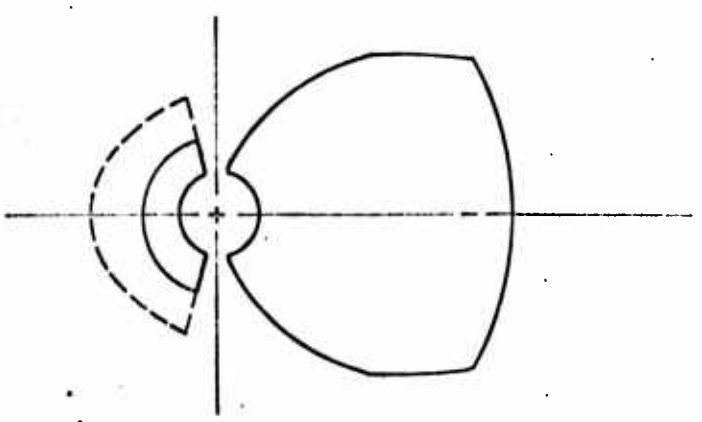

6) Minimum Closing Rate

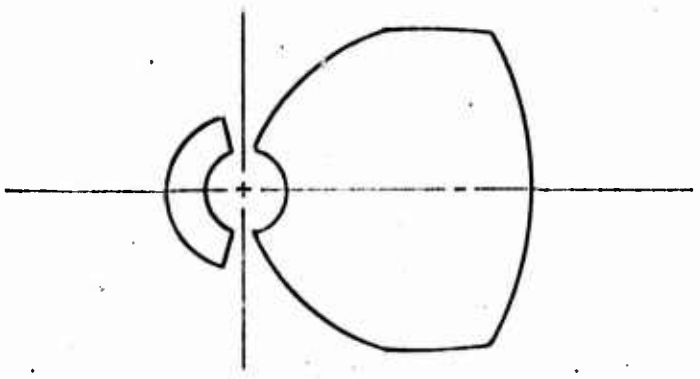

LAR

SECTION 8.0

REFERENCES

1. Locke, Arthur S, Guidance, D. Van Nostrand Co., Princeton, New Jersey, 1955.

2. Bonney, E. A., Zucrow, M. J., and Besserer, C. W., Aerodynamics, Propulsion, Structures and Design Practice, D. Van Nostrand Co., Princeton, New Jersey, 1956.

3. IRE Standards on Radio Aids to Navigation: Definition of Terms, 1954; Proc. IRE, Vol. 43, p 194, February 1955

4. "Simulation of Spikes in AI Radar and Missile Seeker Clutter Spectra (U)", VR 0304C/548, Veda Incorporated, Ann Arbor, Michigan, 10 May 1966, Confidential